ANALYSIS OF THE ABSORPTION PROFILES OF THE COLLISION-INDUCED FUNDAMENTAL BAND OF H_2 IN H_2-Xe, H_2-Kr, AND H_2-Ar MIXTURES

SAMBHU NATH GHOSH

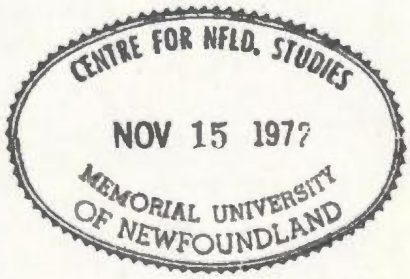
CENTRE FOR NFLD. STUDIES
NOV 15 1972
MEMORIAL UNIVERSITY
OF NEWFOUNDLAND

ANALYSIS OF THE ABSORPTION PROFILES OF THE COLLISION-INDUCED FUNDAMENTAL BAND OF H_2 IN H_2-Xe, H_2-Kr AND H_2-Ar MIXTURES

by

© Sambhu Nath Ghosh, M.Sc. (Calcutta)

Submitted in partial fulfilment
of the requirements for the degree of Master of Science
Memorial University of Newfoundland

September, 1971

CONTENTS

ABSTRACT

The collision-induced fundamental infrared absorpbion band of H_2 was studied at room temperature with an absorption cell of sample path length 105.2 cm in binary mixtures of para H_2 as well as normal H_2 with Xe, Kr, and Ar. The base density of H_2 (para or normal) was in the range 4 - 10 amagat, and the densities of Xe, Kr, and Ar were in the ranges 10 - 70 amagat, 10 - 135 amagat and 10 - 100 amagat, respectively. The prominent feature of the Q branch of the band observed in binary mixtures of pH_2 with all the three perturbing gases is that two dips occur at the Raman frequencies of Q(0) and Q(2) of the low pressure hydrogen gas. The Q branch of pH_2-Xe and that of nH_2-Xe exhibit anomalous intensity distribution, namely, that the Q_P and Q_R peaks show equal intensities.

Profiles for the enhancement of absorption were analyzed by a computational procedure. The quadrupolar components, obtained with para as well as normal H_2, were assumed to have a Boltzmann-modified dispersion line form. The characteristic half-widths δ of the quadrupolar lines in each of the binary mixtures were obtained from the analysis. The present profile analysis reveals that the quadrupolar components show shifts of 9 cm^{-1} in p(or n)H_2-Xe and 6 cm^{-1} in p(or n)H_2-Kr toward lower frequency from the corresponding Raman frequencies of the low pressure gas; it also shows that there is no shift of the quadrupolar components in p(or n)H_2-Ar. The contributions of the quadrupolar and overlap interactions to the total

intensity of the band were derived from the analysis of the profiles in each of the binary mixtures, nH_2-Xe, nH_2-Kr, and nH_2-Ar.

The overlap profiles obtained from the analysis of the experimental profiles of nH_2-foreign gas mixtures were analyzed by a new computational procedure. The line-shape assumed for each of the overlap components consists of two functions; one, the Fourier transform of the intercollisional correlation function given by Van Kranendonk (1968) and the other, the Fourier transform of the intracollisional correlation function given by Levine and Birnbaum (1967). The values of the characteristic inter- and intra-collisional width parameters, δ_D and δ_W, respectively, were derived from the analysis.

The binary and ternary absorption coefficients of the band for nH_2-Ar, nH_2-Kr, and nH_2-Xe were derived. The binary absorption coefficients of the S(0) quadrupolar line, obtained from the profile analysis, were used to calculate the Lennard-Jones molecular diameters σ for H_2-Kr and H_2-Xe molecular pairs.

CHAPTER 1

INTRODUCTION

An isolated homonuclear diatomic molecule in its electronic ground state has no permanent electric dipole moment on account of the symmetry of its charge configuration. Consequently, unlike a polar molecule, it has no electric dipole absorption at its rotational or vibrational frequencies. However, an electric dipole moment can be induced in a colliding pair of molecules by intermolecular forces because of an asymmetric distortion of the charge configuration. This induced dipole moment is modulated by the rotation and vibration of the colliding molecules and by their relative translational motion. As a result, the colliding molecular pair can absorb energy from a radiation field at these frequencies. This phenomenon of collision-induced infrared absorption was first observed by Crawford, Welsh, and Locke (1949) in liquid oxygen and in compressed oxygen in the region of its fundamental vibration-rotation band.

Collision-induced infrared absorption of several molecules has been studied by various researchers since the discovery of this phenomenon. In particular, the fundamental band of gaseous hydrogen has been widely investigated over a variety of experimental conditions. The great interest in the study of this band is due to several reasons: the hydrogen molecule is distinguished by its small moment of inertia, and consequently, its rotational energies are relatively high as compared to those of other molecules and the separation between the adjacent rotational components of

the band is much larger; it is amenable to a theoretical treatment; and furthermore, it remains gaseous over a large range of temperatures, thus making it possible to make measurements over widely different average velocities of the colliding molecular pairs.

Detailed studies of the induced fundamental band of gaseous hydrogen first observed by Welsh, Crawford, and Locke (1949) were made in pure H_2 and in binary mixtures, H_2 - He, H_2 - Ar and H_2 - N_2 at pressures up to 1500 atm in the temperature range 80^oK - 376^oK by Chisholm and Welsh (1954) and at pressures up to 500 atm at 298^oK by Hare and Welsh (1958). Later the band was studied in greater detail by Hunt (1959) in pure H_2 in the temperature range 40^oK - 300^oK and in H_2 - He in the range 85^oK - 300^oK and in H_2 - Ar and in H_2 - N_2 at temperatures 195^oK and 300^oK. Subsequently, Watanabe and Welsh (1965) studied the band in pure H_2 at pressures of the order of 1 atm in the temperature range 18^oK - 77^oK and in H_2 - He at 20^oK. Recently the band was studied at 298^oK in H_2 - Ne and in H_2 - Kr for pressures up to 400 atm by Reddy and Lee (1968) and in H_2 - O_2 and in H_2 - Xe for pressures up to 250 atm by Varghese and Reddy (1969). Very recently a systematic study of the band in H_2 - He and in H_2 - Ne was made by Chang (1971) at four different temperatures in the range 77^oK to 298^oK for gas densities up to 530 amagat.

The observed transitions in collision-induced absorption have been found to obey the Raman selection rules for rotation, i.e. $\Delta J = 0, \pm 2$, J being the rotational quantum number. This is because of the induction mechanism inherent in a molecular collision. Accordingly the induced fundamental band of hydrogen consists of three types of transitions: Q(J) transitions ($\Delta v = 1$, $\Delta J = 0$), S(J) transitions ($\Delta v = 1$, $\Delta J = +2$) and O(J) transitions ($\Delta v = 1$, $\Delta J = -2$). For the fundamental absorption band of

normal hydrogen at room temperature, possible single transitions (see below) are shown in Fig. 1. The vibrational terms $G_0(v)$ and the rotational terms $F_v(J)$ were calculated using the molecular constants of hydrogen obtained by Stoicheff (1957) from the high resolution Raman spectrum of the low-pressure gas.

A theoretical treatment of collision-induced infrared absorption of homonuclear diatomic molecules was given by Van Kranendonk (1957, 1958) using a simplified model for the induced dipole moment by intermolecular interactions. In this model, the induced dipole moment in a binary collision between an absorbing homonuclear diatomic molecule and a perturbing molecule consists of two parts. One part is the short-range electron-overlap dipole moment which decreases exponentially with increasing intermolecular separation R. The other part is the long-range dipole moment resulting from the polarization of one molecule by the quadrupole field of the other and is proportional to R^{-4}. This model is called the exp-4 model. The overlap (isotropic) moment is, to a first approximation, spherically symmetric and independent of the relative orientation of the molecules. It contributes to the intensity of the Q branch (Q overlap) ($\Delta v = 1$, $\Delta J = 0$) which shows a main splitting into two broad components Q_P and Q_R at the lower and higher frequency respectively. The long-range (anisotropic) moment due to quadrupolar induction is strongly dependent on the mutual orientation of the colliding molecules and gives rise to transitions in the O, $Q(Q_Q)$, and S branches. If the perturbing molecule is monatomic, the induced fundamental band consists of only single transitions, but if it has a quadrupole moment, single transitions $O_1(J)$, $Q_1(J)$ and $S_1(J)$ as well as the double transitions $Q_1(J) + S_0(J)$ and $Q_1(J) + Q_0(J)$ occur. Here the subscripts 1 and 0 represent Δv, the change in the vibrational

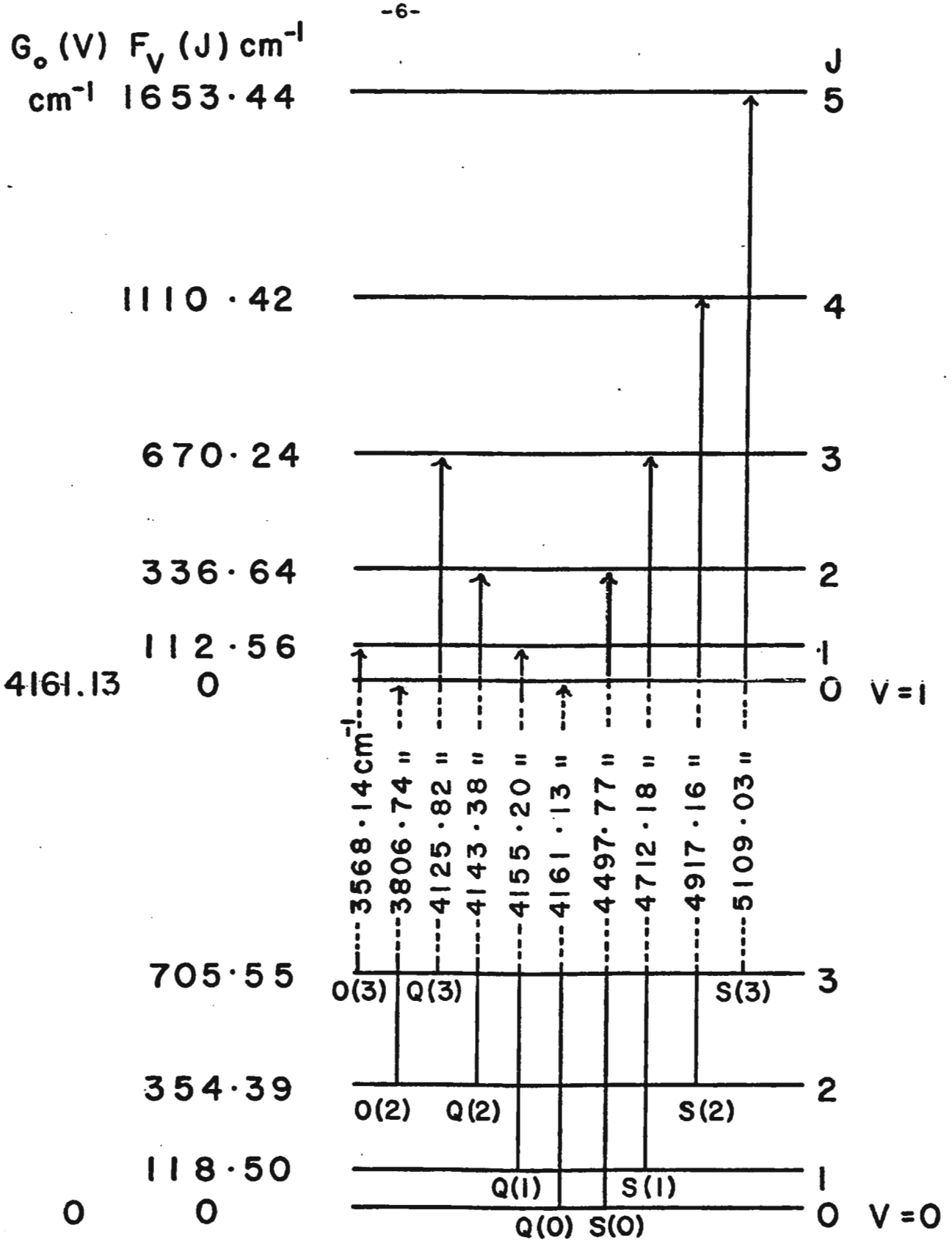

Fig. 1. Single transitions in the collision-induced fundamental band of H_2.

quantum number. In a single transition only one of the colliding pair of molecules makes a vibrational-rotational transition, while the internal energy of the other does not change; in a double transition a single photon is absorbed simultaneously by both the colliding molecules corresponding to a vibrational transition ($Q_1(J)$) in one molecule and a rotational transition ($S_0(J)$) or an orientational transition ($Q_0(J)$ for $J > 0$) in the other molecule.

Figure 2 shows typical enhancement absorption profiles of the fundamental band of normal hydrogen in binary mixtures of hydrogen with argon, krypton, and xenon at room temperature. The positions of the individual lines of the O, Q and S branches as calculated from the known molecular constants of hydrogen (Stoicheff 1957) are marked on the frequency axis. Since the quadrupole moment of each of these perturbing gases is zero, no double transitions occur in the absorption profiles. In these profiles, the Q branch shows a marked dip at the Q(1) Raman frequency (4155 cm^{-1}) with two broad components Q_P and Q_R at lower and higher frequency, respectively. For H_2 - Ar and H_2 - Kr mixtures the Q_R peak is stronger than Q_P. However, the Q branch of the band in H_2 - Xe shows an anomalous intensity distribution, namely that the intensities of the Q_P and Q_R peaks are equal. It was found earlier by Varghese and Reddy (1969) that the separation between the Q_P and Q_R peaks in H_2 - Xe, unlike in other binary mixtures of hydrogen, remains almost constant (approximately 25 cm^{-1}) at all the experimental densities of the mixture. The components of the O, Q and S branches of the band becomes relatively sharper as the perturbing gas becomes heavier. The existence of the quadrupolar component Q_Q in the Q branch of the induced fundamental band of hydrogen has been experimentally observed in pure H_2 and H_2 - Ar and

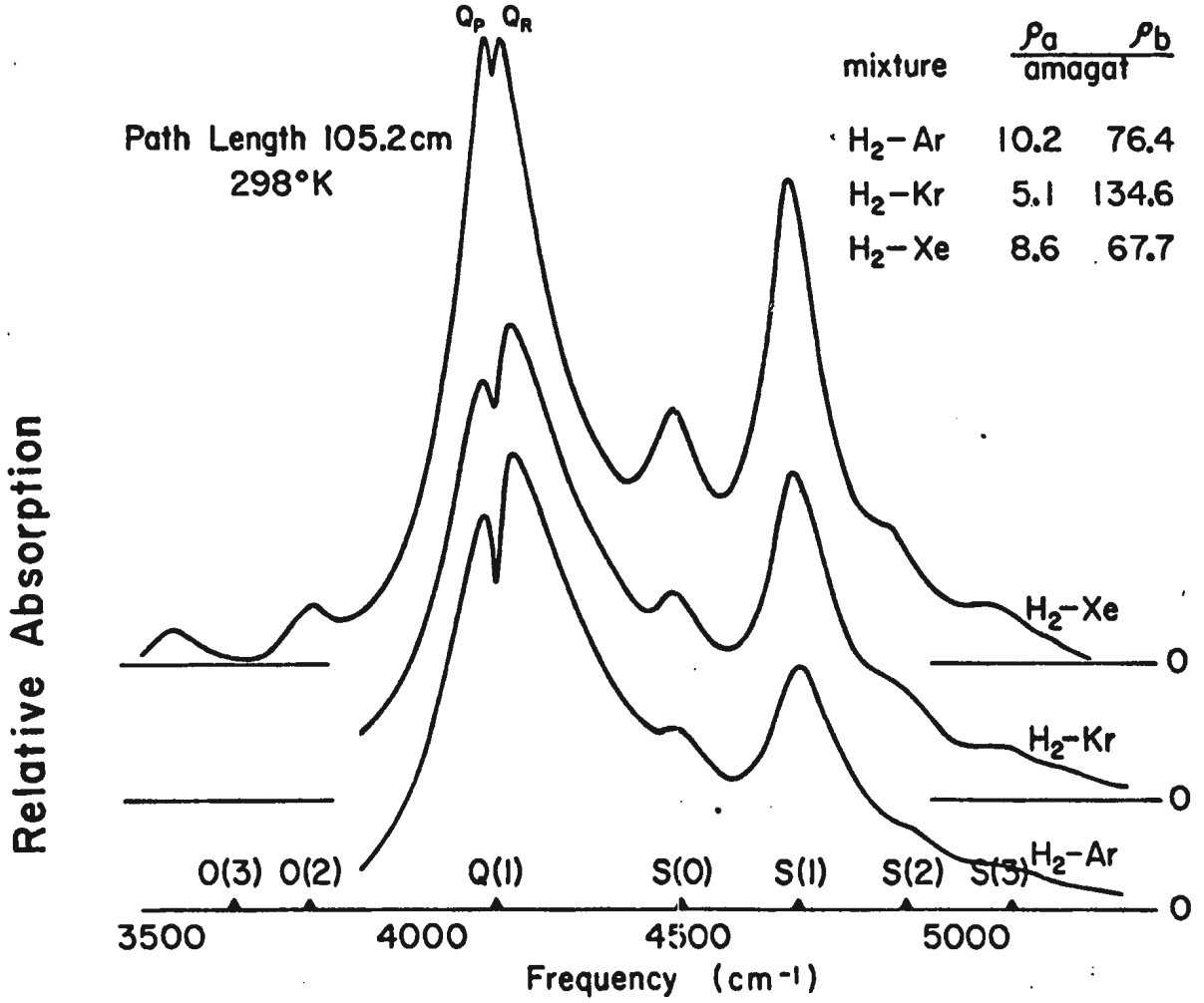

Fig.2. Enhancement absorption profiles of the induced fundamental band of H_2 in nH_2-Ar, nH_2-Kr, and nH_2-Xe mixtures.

H_2 - N_2 mixtures at high pressures by Hare and Welsh (1958) and in H_2-Kr mixtures at moderate pressures by Reddy and Lee (1968). It has also been observed in pure hydrogen at low pressures by Watanabe and Welsh (1967).

Up to moderately high pressures, collision-induced absorption is produced mainly by binary collisions between molecules. Only at very high pressures, ternary and higher order collisions contribute a considerable amount to the total absorption. In the former case the absorption lines retain more or less a constant shape. The broad appearance of the collision-induced spectra is due to the participation of the relative translational energy of the colliding molecules in the absorption process. This participation causes a line of molecular frequency ν_m (cm^{-1}) to have a frequency distribution consisting of summation and difference tones $\nu_m \pm \nu_{tr}$, where ν_{tr} is the continuum of frequencies (cm^{-1}) corresponding to possible changes in the relative translational energy of the colliding pair of molecules. The intensities in the low- and high- frequency wings of the lines in collision-induced spectra are therefore expected to be connected by the Boltzmann relation. This is recognized for the Q branch of the induced fundamental band of hydrogen in H_2 - He by Chisholm and Welsh (1954) and for the induced rotational spectrum of H_2 by Kiss and Welsh (1959).

The first profile analysis of collision-induced spectra was made by Kiss and Welsh (1959) who used a Boltzmann-modified dispersion line shape (see Chapter 3) for the individual transitions in the pure rotational spectrum of hydrogen at low temperatures and found good agreement between the experimental profiles and the calculated profiles. Profile analysis of the induced fundamental band of hydrogen was first attempted by Hunt and Welsh (1964) who showed that the Q_R component could be represented by a dispersion line shape and the quadrupolar S(J)

lines could also be represented by the Boltzmann-modified dispersion line shape. In this analysis these authors neglected the dip of the Q branch whose origin was not understood at that time.

Bosomworth and Gush (1965) investigated the line profiles of the pure translational absorption down to 20 cm^{-1} at 295°K in the rare gas mixtures and in hydrogen and of the pure rotational absorption in hydrogen at 300°K and 77°K. They found that the dispersion line form gave too much intensity in the tail of an individual line. A better fit of the synthetic profile to the experimental profile was obtained by them by attaching an exponential tail to the dispersion line form. Recently Mactaggart and Hunt (1969) introduced a power-law tail to the dispersion line form and obtained a much better representation of the experimental data on the high-frequency wing of the pure rotational spectrum of hydrogen.

Watanabe and Welsh (1967) analyzed the absorption profiles of the induced fundamental band of hydrogen in the pure gas at low densities and at low temperatures. These authors found that both the overlap and quadrupolar components could be represented by a Boltzmann-modified dispersion line form. They also found that an enhancement absorption profile of the band in H_2 - He at 20°K could be represented by a dispersion line shape with an exponentially decreasing tail. For molecular hydrogen, theoretical calculations of the matrix elements of the quadrupole moment and of the polarizability were made by Karl and Poll (1967) and by Kolos and Wolniewicz (1967), respectively. The calculated quadrupole matrix elements were found to be strongly dependent on the rotational quantum numbers of the initial and final states of the transitions. Making use of these matrix elements of the quadrupole moment and of the polarizability, Watanabe (1971) reanalyzed the induced infrared absorption spectra of

hydrogen in the pure gas in the fundamental region, recorded at 18°K, 20.4°K and 24°K.

The empirical line shapes discussed above do not reproduce the splitting of the Q branch of the induced fundamental band into the overlap components Q_P and Q_R. Van Kranendonk (1968) showed that the observed dip in the Q branch is due to a destructive interference of the radiation process which occurs as a result of the negative correlations existing between the short-range (isotropic) parts of the dipole moments induced in successive collisions. A similar dip was predicted by Van Kranendonk to exist in the translational spectra of inert gas mixtures at zero frequency. Levine and Birnbaum (1967) in an attempt to obtain a theoretical line shape for the pure translational spectra used a Gaussian-type dipole moment rather than a pure exponential form related to the overlap interaction (in the exponential-4 model of Van Kranendonk); this dipole moment $\to 0$ as the intermolecular separation $R \to 0$. Levine and Birnbaum calculated an intracollisional line shape in the form of a modified Bessel function of the second kind. (Note that the terms 'intracollisional' and 'intercollisional' refer respectively to single collisions and successive collisions). Sears (1968) calculated the translational line shape function classically, assuming an isotropic model for the induced dipole moment and a Lennard-Jones potential for the colliding pairs of molecules. Quantitative expressions given by Van Kranendonk (1968) and Levine and Birnbaum (1967) will be discussed later in Chapter 3 of this thesis.

The present investigation was designed to obtain reasonably accurate enhancement absorption profiles of the fundamental band of hydrogen in binary mixtures of parahydrogen as well as normal hydrogen with argon, krypton and xenon at room temperature and to make an analysis

of these profiles. One of the aims of the present study is to understand the anomalous intensity distribution of the Q branch of the band in H_2 - Xe mixtures. Chapter 2 of this thesis gives an account of the apparatus and the experimental procedure used in the present study. The experimental enhancement absorption profiles, their analysis, and the results obtained from it are presented in Chapter 3. In Chapter 4, absorption coefficients are derived and Van Kranendonk's theory is applied to the present experimental results.

CHAPTER 2

APPARATUS AND EXPERIMENTAL METHOD

To study the enhancement absorption profiles of the collision-induced fundamental band of hydrogen in binary mixtures of hydrogen with argon, krypton and xenon at room temperature a 1 m transmission-type absorption cell was used. Both para and normal hydrogen were used as the base gas. Conversion of normal hydrogen to parahydrogen was achieved in a specially constructed apparatus. The maximum experimental pressures reached were 1550 p.s.i, 1900 p.s.i, and 800 p.s.i with the perturbing gases argon, krypton and xenon respectively. Perkin-Elmer Model 112 single-beam double-pass spectrometer with a LiF prism and a PbS detector was used to record the spectra. A description of the apparatus and the experimental procedure adopted in its use is presented in this chapter.

2.1 The 1 m Absorption Cell

This cell is of the transmission-type and was described previously by Bishop (1966) and Chang (1971). The sample path length of the cell at room temperature was 105.2 cm. The cell was tested for pressures up to 400 atm at room temperature. Its construction details are shown in Fig. 3.

The cell body A is a 303 stainless steel tube, 1 m long, 3/4 in. in inner diameter and 1.0 in. in outer diameter. The stainless steel flange F was hard-soldered to the cell at each of its ends. Each of the end pieces B, also made of 303 stainless steel, 5 in. long and 3 in. in

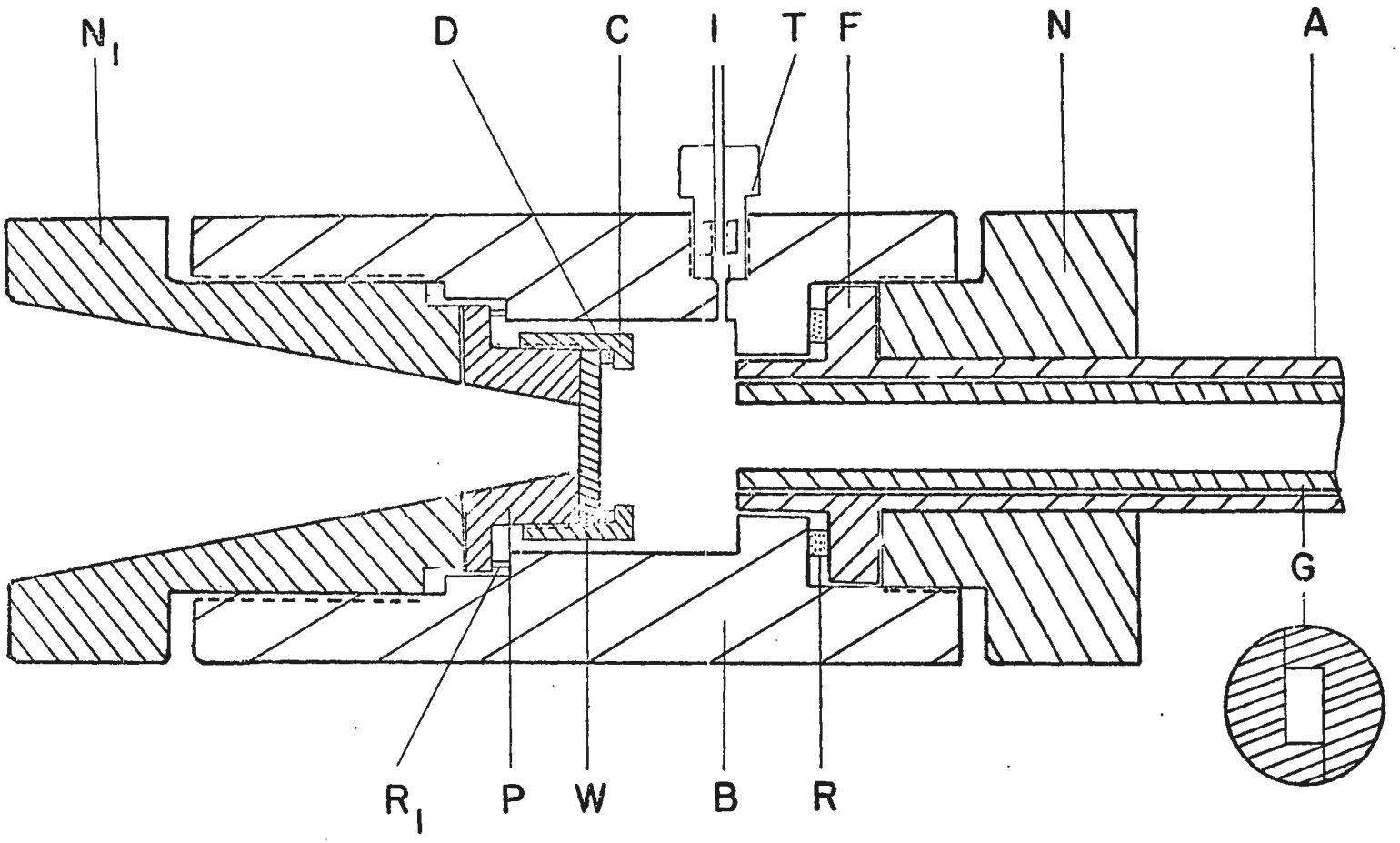

Fig.3. The 1m absorption cell (a cross-section of one end is shown).

diameter, was attached to the cell body A by means of the steel closing nut N. A stainless steel ring R between the flange F and the end piece B provided a pressure-tight seal between the cell body and the end piece. A stainless steel light guide G whose inner surfaces were polished to give a high reflectivity of the incident radiation was made in four sections and has a central rectangular aperture 0.4 in. x 0.2 in. Each section of the light guide consisted of two lengthwise parts. A locking arrangement, provided between adjacent sections of the light guide, prevented their misalignment.

Each of the optically flat synthetic sapphire windows W, 1.0 in. in diameter and 5 mm thick, was cemented on to the optically flat stainless steel plate P by means of a thin layer of General Electric RTV-108 silicone rubber cement. These window plates P have rectangular apertures 0.5 in. x 0.2 in. Two steel caps C with teflon rings D secured the windows to the window plates, thus preventing the windows from becoming loose during evacuation. A pressure-tight seal between the window plate P and the end piece B was obtained by closing the steel nut N_1 with a teflon ring R_1. The outer portion of the window plate P was made into a square so that it fits into a matched square recess of the end piece B, thus preventing misalignment of the window plate with respect to the light guide while tightening the nut N_1. A 1/4 in. diameter stainless steel capillary tube I which was connected to the end piece B by means of an Aminco fitting T served as a gas inlet to the absorption cell.

2.2 Ortho-Para Hydrogen Conversion Mechanism

Molecular hydrogen exists in two distinct modifications, the ortho-hydrogen and the parahydrogen. In the ortho modification, the nuclear spins of

the individual hydrogen atoms (the nuclear spin quantum number of each atom, I = 1/2) are oriented in the same direction (parallel) giving the total nuclear spin quantum number T = 1, whereas in the para modification these are oriented in opposite directions (antiparallel) giving T = 0. Even T values are possible for symmetric rotational levels, J = 0, 2, 4, . . . , and odd T for antisymmetric levels, J = 1, 3, 5, . . . , J being the rotational quantum number. Correspondingly, in molecular hydrogen, even and odd rotational levels are, respectively, occupied by para and ortho molecules. At thermal equilibrium, the individual distributions of the para and ortho molecules in various rotational levels are calculated from (i) the (2T + 1) - fold degeneracy of the rotational levels due to nuclear spin, (ii) the (2J + 1) - fold degeneracy of the rotational levels, and (iii) the Boltzmann distribution law. The ortho-para ratio of molecular hydrogen is determined by the number of molecules occupying odd or even rotational states, respectively. When the temperature is changed, the equilibrium energy distribution of the molecules is also changed. However, under normal conditions, transitions between ortho and para modifications are forbidden because of the selection rule 'antisymmetric $\leftrightarrow\!\!\!\!\!\!+\!\!\!\!\!\!\rightarrow$ symmetric'. When normal hydrogen is cooled to a very low temperature, molecules which were originally in odd numbered rotational levels go to the state J = 1. Consequently, distribution of rotational levels at that temperature does not correspond to thermal equilibrium. However when the gas is kept at that very low temperature for a sufficiently long time, all the molecules will, eventually, go to the lowest energy state J = 0.

There are two basic methods of inducing an ortho-para transition. One method consists of dissociating hydrogen molecules into atoms and then

allowing the atoms to recombine. Upon dissociation of the atomic state, nuclear spins of hydrogen atoms are randomly oriented. When they are reunited, molecules are formed according to the equilibrium energy distribution determined by the temperature. The second method involves the interaction of the nuclear magnetic moment of hydrogen molecules with an extermal inhomogeneous magnetic field of molecular dimensions. The inhomogeneous external magnetic field interacts with the nuclear spin magnetic moment of one of the atoms of the molecule and causes a spin reversal, thus in effect inducing an ortho-para transition.

Effective ortho-para hydrogen conversion is most suitably achieved at low temperatures by using a heterogeneous catalyst. The transition from the ortho to the para state is brought about by the influence of the inhomogeneous magnetic field of the paramagnetic component of the heterogeneous catalyst upon the physically adsorbed hydrogen on the catalyst surface (see, for example, Schmauch and Singleton, 1964).

In the next section of this chapter we describe an apparatus designed for the ortho-para hydrogen conversion. In this apparatus we made use of APACHI 1 ($NiO.\ 2{\cdot}5\ SiO_2$) ortho-parahydrogen conversion catalyst at a low temperature. APACHI 1 (Air Products And CHemicals Inc.) has a high adsorptive capacity for hydrogen, a high concentration of a paramagnetic component on the surface of the catalyst and a large magnetic moment associated with the paramagnetic component. Schmauch and Singleton (1964) have claimed that APACHI 1 showed a tenfold increase in conversion activity, on a weight basis, over the widely used hydrous ferric oxide gel catalysts in the past.

2.3 The Apparatus for the Conversion of Normal Hydrogen to Parahydrogen

The apparatus constructed for the purpose of conversion of normal hydrogen to parahydrogen is schematically shown in Fig. 4. It consists essentially of three long-stemmed bulbs A, B and C. A is the conversion bulb made of pyrex glass and was filled upto 1/3 of its volume with the catalyst 'APACHI 1', a free sample of which was supplied by Houndry process and Chemical Company, Philadelphia. B and C were made of copper. The bulbs A and B were connected to valves V and V' through the flexicoils K and K' and were maintained in a liquid He dewar. All the three bulbs were interconnected through valves, V, V' and V_3 and the pressure gauge G was connected in between V_3 on one side and V and V' on the other. The system was connected to a Matheson 'ultra high purity' hydrogen cylinder and to a vacuum pump through a two way valve V_1 - V_1' and another valve V_2. The flexicoils K and K' enable the bulbs A and B to be raised above or lowered below the level of liquid helium.

For conversion of normal hydrogen to parahydrogen the procedure described below was adopted. First the entire system was evacuated and the valves V_2, V and V' were closed. Normal hydrogen from the cylinder was introduced into the bulb C at a pressure of approximately 1200 p.s.i. at room temperature, which was later cooled by liquid nitrogen. Valves V_1, V_2 and V_3 were closed and the bulb A was then lowered into liquid helium. By carefully operating the valves V_3 and V in several steps sufficient quantity of hydrogen was slowly solidified in bulb A. Valve V was then closed. After the rest of the system was evacuated valves V_2 and V_3 were closed. Valve V was then opened and A was carefully raised above the liquid helium level so that the solidified hydrogen slowly converted itself

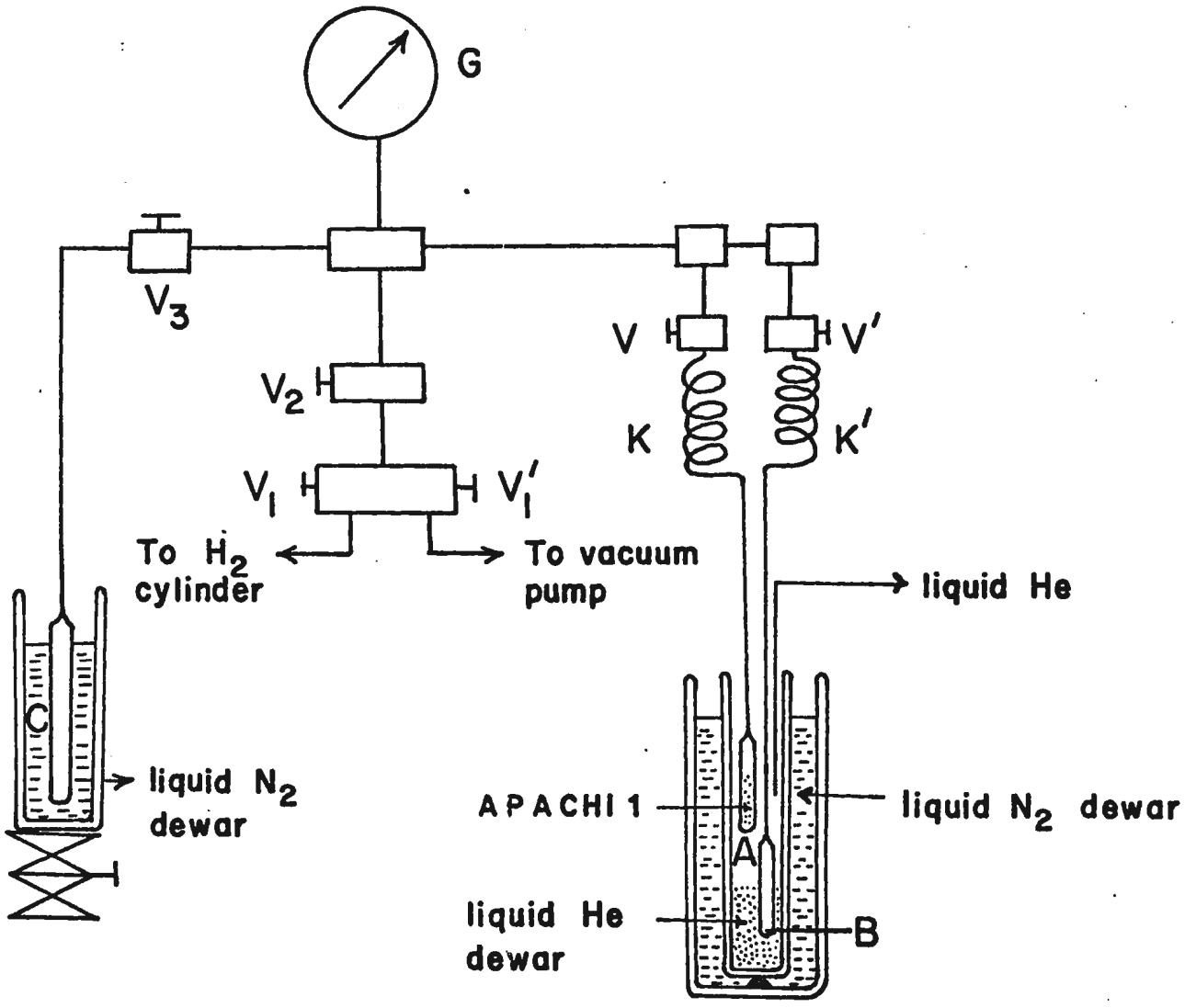

Fig.4. A schematic diagram of the ortho-para hydrogen conversion apparatus.

into liquid. By carefully adjusting the height of the bulb A in the liquid helium dewar hydrogen was kept in liquid state in contact with the catalyst for a period of about half an hour. The conversion of normal hydrogen to parahydrogen took place during this period. Valve V' was then opened. By lowering the copper bulb B into liquid helium and raising bulb A further in the dewar, para-enriched hydrogen from A was boiled off and then condensed into B. Finally liquid helium in the dewar was allowed to boil off and para-enriched hydrogen was carefully collected into the copper bulb C which was cooled with liquid nitrogen.

2.4 The Optical Arrangement

A schematic representation of the optical arrangement used with the 1 m absorption cell is shown in Fig. 5. The source S was a water-cooled tungsten-filament lamp with a sapphire window, prepared from a General Electric 750 watt projection-bulb filament (Kuo 1970). It was operated at a power of approximately 250 watts obtained from a stabilized a.c. power unit which was in turn fed from a Sorenson a.c. power regulator, Model ACR-2000. Radiation from the source was first focussed on the entrance window of the absorption cell H by means of a front-surface aluminized spherical mirror M_1 and that from the exit window of the cell was then focussed by a similar mirror M_2 on to the slit S_1 of a Perkin-Elmer Model 112 single-beam double-pass prism spectrometer A. The spectrometer was equipped with a LiF prism and a PbS detector operated at room temperature. F/4 light cones were used throughout the optical arrangement.

Since strong absorption of atmospheric water vapor overlaps both the low- and high-frequency ends of the fundamental band of hydrogen, the level of the water vapor in the optical path was maintained at a minimum

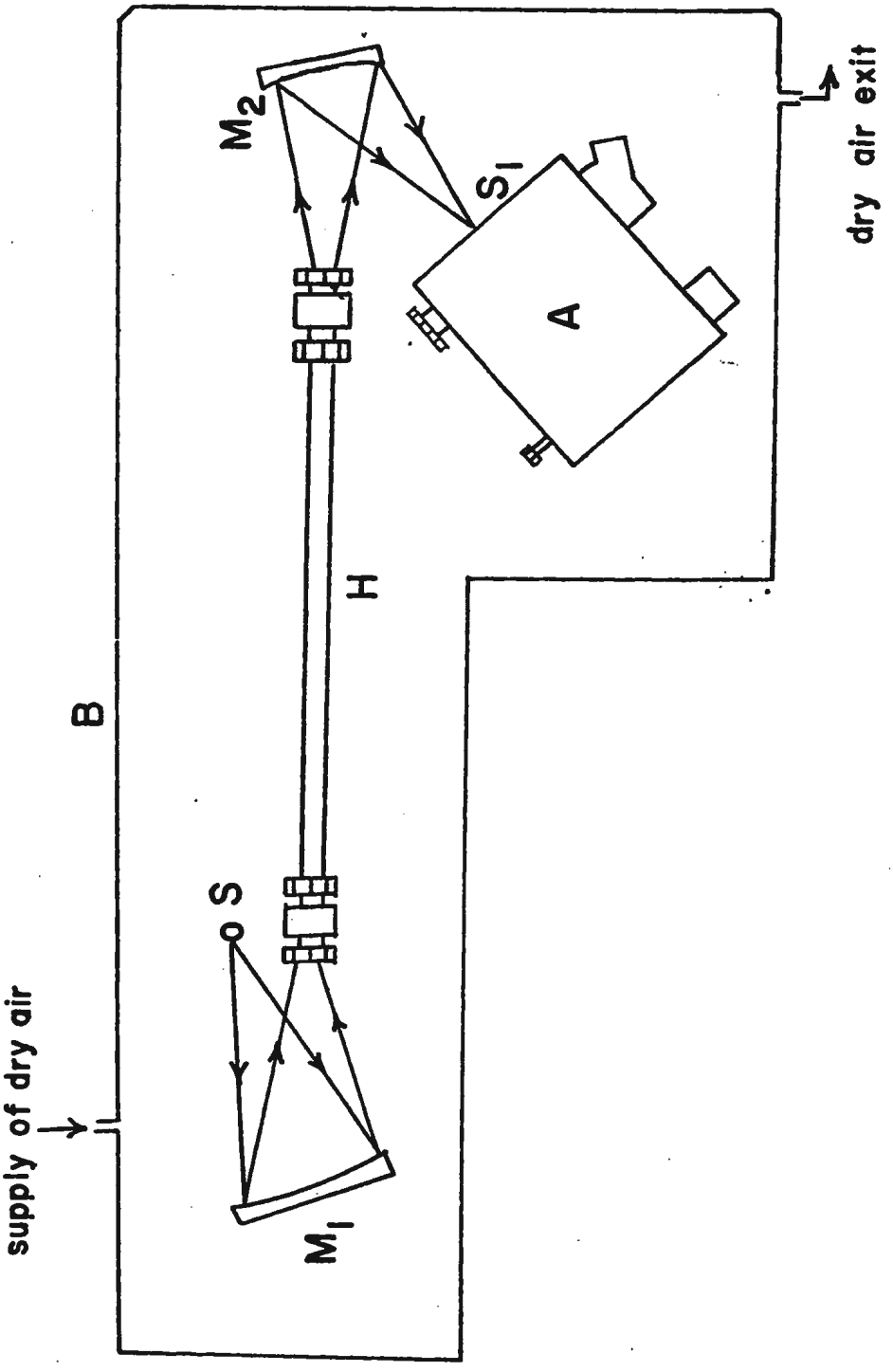

Fig.5. The optical arrangement.

by the following method. The whole optical system including the source and spectrometer was kept in a polyethylene enclosure B and dry air was flushed continuously through the enclosure. Dry air was obtained by passing compressed air through a series of liquid nitrogen , molecular sieve , and phosphorus pentoxide traps.

The slit width of the spectrometer was set at 50 μ, which gave a spectral resolution of approximately 4 cm^{-1} at the origin (4161 cm^{-1}) of the fundamental band of hydrogen.

2.5 The Gas Handling System

Figure 6 shows schematically the gas handling system used in the present experiments. Here G_1, G_2 and G_3 are Bourdon tube pressure gauges in the ranges 0 - 5000 p.s.i., 0 - 3000 p.s.i. and 0 - 160 p.s.i., respectively, which were calibrated against an Ashcroft dead-weight pressure balance having an accuracy of greater than 1%. V_1 to V_8 are Aminco high pressure valves, C is a liquid nitrogen trap made of copper tubing, 1/4 inch in outside diameter, T_1 and T_2 are stainless steel thermal compressors, and H is the absorption cell. Stainless steel capillary tubing, 1/4 inch in outside diameter was used to connect different components of the gas handling system. The assembled system was tested for pressures up to 3000 p.s.i. and for good vacuum.

In the present experiments Matheson 'ultra high purity' normal hydrogen (or para-enriched hydrogen prepared in our laboratory, see section 2.3) and argon and Matheson research grade xenon and krypton were used. For each mixture experiment hydrogen gas was admitted into the evacuated absorption cell H through the liquid nitrogen trap C, with the valve V_4 closed. The base pressure of hydrogen was read on the low range gauge G_3.

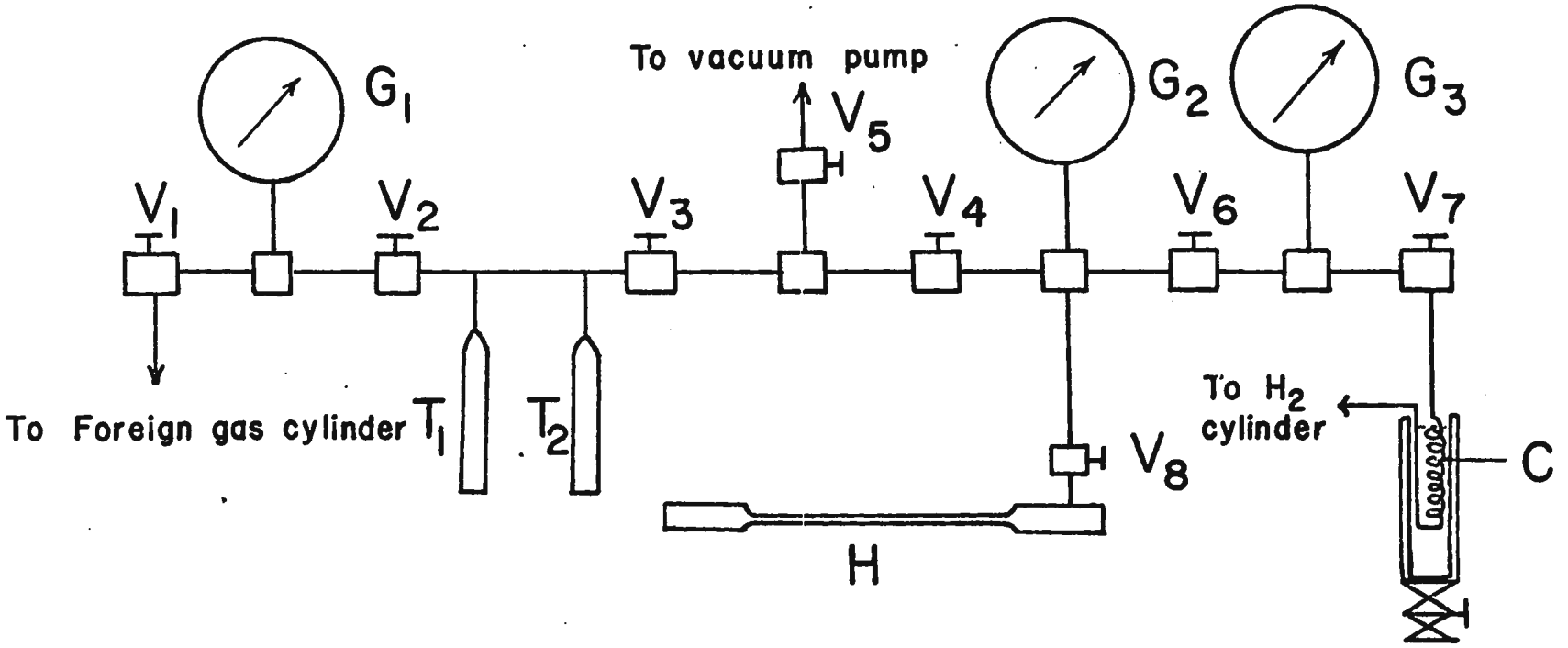

Fig.6. The gas handling system.

Recorder traces of the transmitted intensity I_1 by the cell for a given base pressure of hydrogen were recorded until they were reproducible. The valves V_6 and V_8 were then closed and the system was re-evacuated. To obtain the required pressures of xenon, krypton or argon thermal compressors T_1 and T_2, cooled initially by liquid nitrogen and allowed subsequently to warm up, were used. The perturbing gas was admitted into the absorption cell at the required pressures in sharp pulses by means of valve V_8. The pressure of gas mixture in the cell was read on gauge G_2. For each pressure of the mixture, spectrometer traces of intensity I_2 were taken until a satisfactory reproduction was obtained. In the present experiments the base density of hydrogen (normal or para) was in the range 4 to 10 amagat and the density of the perturbing gas was in the range 15 to 50 amagat for xenon, 18 to 75 amagat for krypton and 50 to 100 amagat for argon.

Since krypton and xenon are expensive, each of these gases was recovered, after the completion of a mixture experiment with a constant base density of hydrogen, by the following cryogenic method. The perturbing gas from the mixture was condensed into its original cylinder, cooled with liquid nitrogen. The hydrogen gas was then slowly let out of the system which was later evacuated. The solidified krypton or xenon was then allowed to evaporate in its cylinder. The procedure of solidification, evacuation and evaporation was repeated several times. It was made sure that these gases were free from any trace of hydrogen by checking the absorption of compressed krypton or xenon in the absorption cell at the required high pressure in the spectral region of the fundamental band of hydrogen.

2.6 Calibration of the Spectral Region and Reduction of Experimental Traces

The spectral region from 3500 cm^{-1} to 6000 cm^{-1} was calibrated

with the known frequencies of Hg-emission lines (Humphreys 1953; I.U.P.A.C. Tables of Wave Numbers 1961) and absorption peaks of atmospheric water vapor (Benedict and Plyler 1951; I.U.P.A.C. Tables of Wave Numbers 1961) and 1, 2, 4 - trichlorobenzene (Plyler, Blaine and Nowak 1957). A computer program was used to obtain a smooth curve through the points on a graph of frequency against position on the recorder trace. The details of the procedure used are as follows: The distances of the standard emission and absorption peaks were accurately measured from a reference water vapor absorption peak at 3852.1 cm^{-1} on the recorder charts. These distances $d(\nu)$ were then expressed as a polynomial function of frequency (cm^{-1}) ν of the peaks in the form,

$$d(\nu) = A + B\nu + C\nu^2 + D\nu^3 + E\nu^4 + F\nu^5 .$$

A least squares fit was obtained to calculate the constants A to F with the help of IBM 360/40 computer, and these constants were in turn used to obtain frequency against position on a recorder trace at 5 or 10 cm^{-1} intervals. A calibration chart was then drawn on a tracing paper giving the position along the recorder trace at these intervals. This chart was positioned on the recorder trace using water vapor peaks at 3852.1 and 5141.7 as reference peaks.

To obtain experimental traces the gain of Model 107 amplifier of the Perkin-Elmer spectrometer was first adjusted until the recorder pen had 95% of the full scale deflection at 5600 cm^{-1} with the radiation from the source passing through the evacuated absorption cell. The balance point of the potentiometer circuit of the amplifier was then adjusted such that the infinite absorption line corresponding to the cut off of radiation from the source coincided with the zero-line of the recorder chart.

In the present experiments, the enhancement of absorption of the

fundamental band of hydrogen, when the perturbing gas argon, krypton or xenon was admitted at different pressures into the absorption cell containing a fixed base pressure of hydrogen (normal or para) was of prime interest. $\alpha_{en}(\nu)$, the enhancement in the absorption coefficient per unit path length at a given frequency $\nu(cm^{-1})$ due to addition of a perturbing gas at a density ρ_b into the absorption cell containing an absorbing gas at a fixed base density ρ_a is given by the relation

$$\alpha_{en}(\nu) = (2.303/\ell) \log_{10} (I_1(\nu)/I_2(\nu)),$$

where ℓ is the sample path length of the cell, $I_1(\nu)$ is the intensity transmitted by the absorbing gas in the cell at ν, and $I_2(\nu)$ is the intensity transmitted by the binary gas mixture in the cell at the same frequency ν. The spectrometer traces obtained in a mixture experiment at different pressures of the perturbing gas were plotted on the trace obtained with the corresponding base pressure of hydrogen. The calibration chart prepared earlier was then positioned on the latter trace and the enhancement in absorption was measured with the help of a standard logarithmic scale by measuring $\log_{10} (I_1/I_2)$ at intervals of 5 cm^{-1} in the regions of the band origin and the S branch peaks and at intervals of 10 cm^{-1} in the rest of the spectral region of the band. The enhancement absorption profiles were obtained by plotting $\log_{10} (I_1/I_2)$ against ν.

2.7 Isothermal Data of the Experimental Gases

The density of a gas expressed in units of amagat (which is defined as the ratio of the density of a gas at a given temperature and pressure to its density at S.T.P.) is directly related to its number density (i.e. the number of molecules per unit volume). In collision-

induced absorption it is customary to express densities of gases in amagat units.

The base density ρ_a of hydrogen (it is assumed that the densities of normal and para varieties are the same under similar conditions of temperature and pressure) is directly obtained from its isothermal data given by Michels, De Graaff, Wassenaar, Levelt and Louwerse (1959). The following references were used to obtain the isothermal data of the perturbing gases: Michels, Boltzen, Friedman and Sengers (1956) for argon, Trappeniers, Wassenaar and Wolkers (1966) for krypton, and Michels, Wassenaar and Louwerse (1954) for xenon.

The partial density ρ_b of the perturbing gas in a binary mixture was determined from the formula (see for example, Reddy and Cho 1965)

$$\rho_b = \{1/(1 + \beta)\}\{(\rho_a)_p + \beta(\rho_b)_p\} - \rho_a ,$$

where $(\rho_a)_p$ is the density of hydrogen at the total pressure P of the mixture and $(\rho_b)_p$ is the density of the perturbing gas at the same pressure, and $\beta = \rho_b'/\rho_a$ where ρ_b' is the approximate partial density of the perturbing gas corresponding to the partial pressure $P_b = P - P_a$, P_a being the pressure of hydrogen. The final value of ρ_b was determined by the method of successive iterations.

CHAPTER 3

ANALYSIS OF THE ENHANCEMENT ABSORPTION PROFILES OF THE COLLISION-INDUCED FUNDAMENTAL BAND OF H_2

Accurate enhancement absorption profiles of the collision-induced fundamental band of hydrogen in binary mixtures of parahydrogen as well as normal hydrogen with argon, krypton, and xenon were obtained at 298^{o}K with an absorption cell of sample path length 105.2 cm using the experimental apparatus described in the previous chapter. In the present experiments the base density of hydrogen (para as well as normal) was in the range 4 to 10 amagat and the densities of the perturbing gases xenon, krypton, and argon were in the ranges 10 to 70 amagat, 10 to 135 amagat and 10 to 100 amagat, respectively. In the density ranges used here, binary collisions between the hydrogen molecules and the perturbing gas molecules produce almost the entire absorption of the band while the ternary (and higher order) collisions contribute a negligible amount. The enhancement absorption profiles obtained with para-enriched hydrogen as the base gas correspond to a parahydrogen concentration of 90%. At room temperature, the first four rotational levels J = 0 to 3 of the ground vibrational state are populated in normal hydrogen, whereas only two rotational levels J = 0 and 2 are populated in parahydrogen. Consequently, the induced fundamental band of parahydrogen is simpler than that of normal hydrogen. In the following sections we first present the experimental enhancement absorption profiles of the fundamental band of parahydrogen in the binary mixtures, pH_2 - Xe, pH_2 - Kr and pH_2 - Ar, and an analysis of

these profiles; in the latter sections of this chapter we present an analysis of the enhancement absorption profiles of the fundamental band of normal hydrogen in the binary mixtures, nH_2 - Xe, nH_2 - Kr and nH_2 - Ar.

3.1 Experimental Enhancement Absorption Profiles of pH_2 - Xe, pH_2 - Kr and pH_2 - Ar.

Figures 7, 8, and 9 show typical sets of experimental profiles for the enhancement of absorption of the band at room temperature in binary mixtures of parahydrogen (90% para) with xenon, krypton, and argon, respectively; in each figure, two profiles for a particular base density of parahydrogen and for two different densities of a perturbing gas are shown. The value of $\log_{10}(I_1/I_2)$ was plotted against frequency (cm^{-1}) in all the figures. The positions of Raman frequencies, 4143.4 (Q(2)), 4161.1 (Q(0)), 4497.8 (S(0)), 4712.9 (S(1)) and 4917.2 cm^{-1} (S(2)), as obtained from the constants of the low pressure hydrogen gas (Stoicheff, 1957) are marked in these figures. The prominent feature of the Q branch in Figs. 7 to 9 is that two sharp dips occur at the Raman frequencies of Q(0) and Q(2) of the low pressure gas. This observation, together with the observation of dips at Q(1) and Q(3) frequencies of the band in mixtures of normal hydrogen and neon by Reddy and Lee (1968), clearly establishes the fact that each of the components $Q_{overlap}$ (J) has a dip at the corresponding molecular frequency Q(J). Varghese and Reddy (1969) reported that the Q branch of the fundamental band of H_2 in mixtures of normal hydrogen and xenon shows an anomalous intensity distribution, namely, that the intensities of the Q_P and Q_R peaks are equal and the separation between them remains almost constant at all the experimental densities of the mixtures. The profiles of pH_2 - Xe in Fig. 7 also show a similar anomalous

Fig.7. Enhancement absorption profiles of the induced fundamental band of H_2 in pH_2-Xe mixtures.

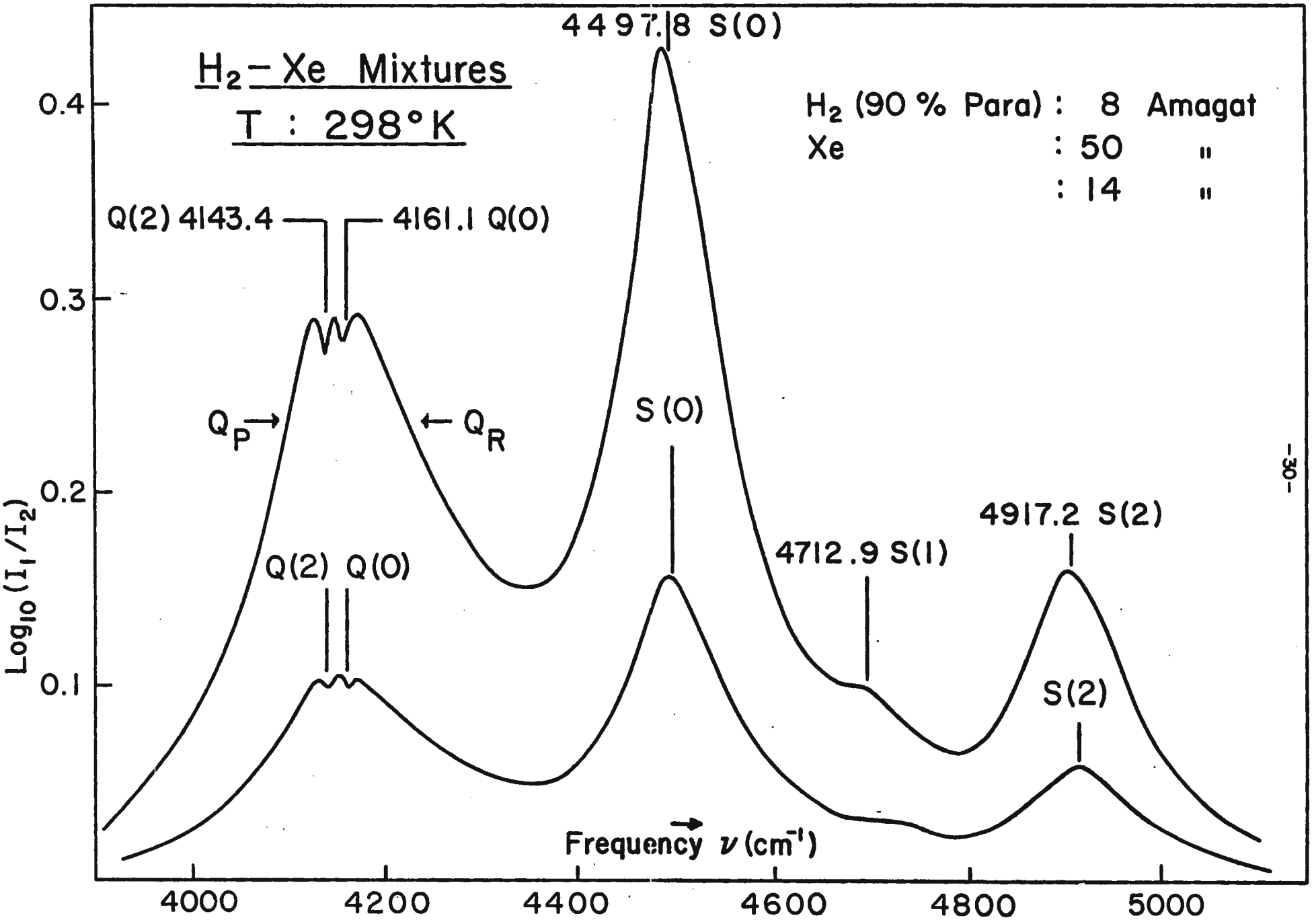
H2 – Xe Mixtures
T : 298°K
H2 (90 % Para) : 8 Amagat
Xe : 50 "
: 14 "
4497.8 S(0)
Q(2) 4143.4
4161.1 Q(0)
QP
QR
S(0)
Q(2) Q(0)
4712.9 S(1)
4917.2 S(2)
S(2)
Log10 (I1/I2)
0.4
0.3
0.2
0.1
Frequency ν (cm-1)
4000
4200
4400
4600
4800
5000

Fig.8. Enhancement absorption profiles of the induced fundamental band of H_2 in pH_2-Kr mixtures.

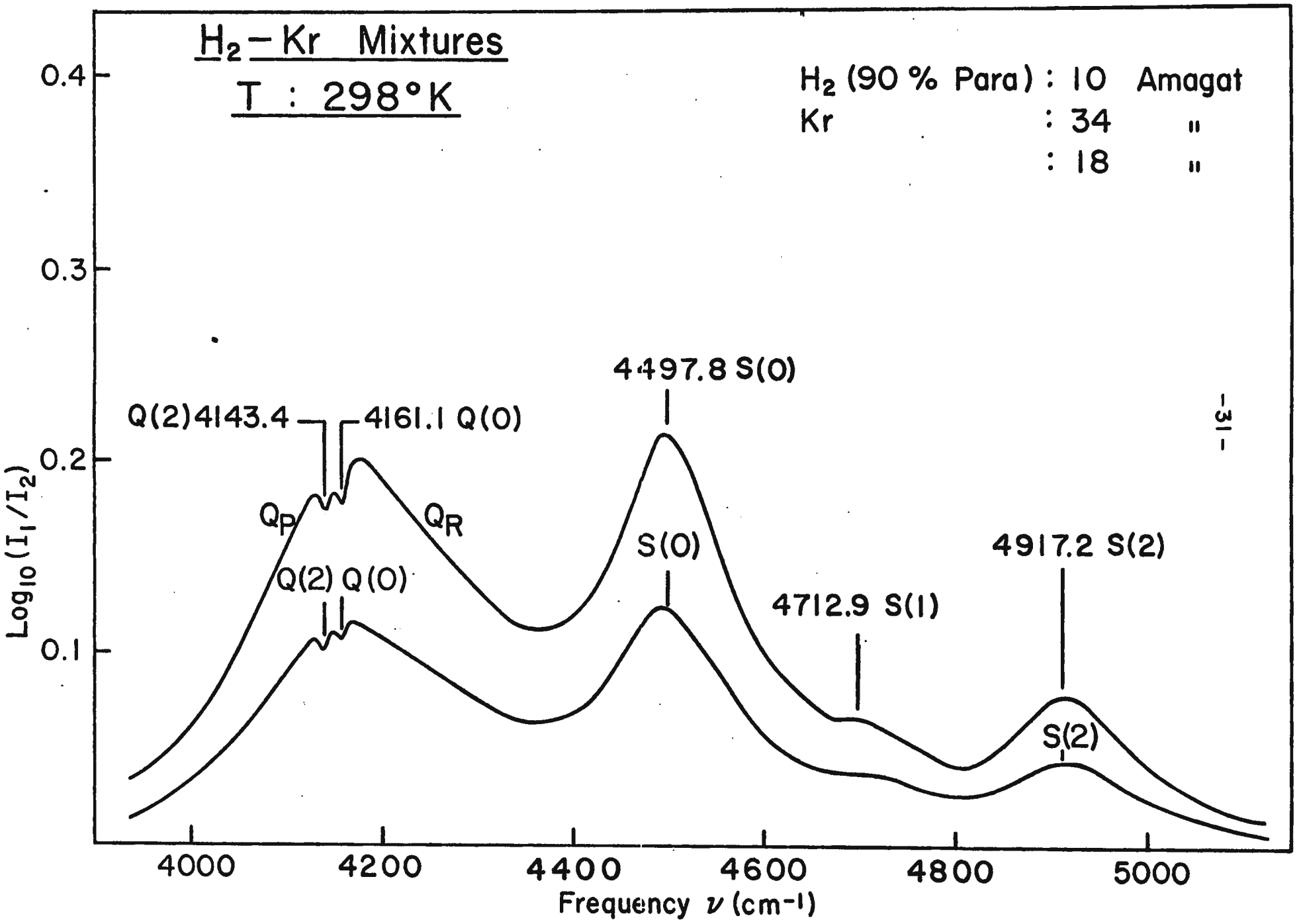
H2 – Kr Mixtures
T : 298°K
H2 (90 % Para) : 10 Amagat
Kr : 34 "
: 18 "
0.4
0.3
0.2
0.1
Log10 (I1/I2)
Q(2)4143.4
4161.1 Q(0)
4497.8 S(0)
QP
QR
Q(2) Q(0)
S(0)
4712.9 S(1)
4917.2 S(2)
S(2)
4000
4200
4400
4600
4800
5000
Frequency ν (cm-1)

Fig.9. Enhancement absorption profiles of the induced fundamental band of H_2 in pH_2-Ar mixtures.

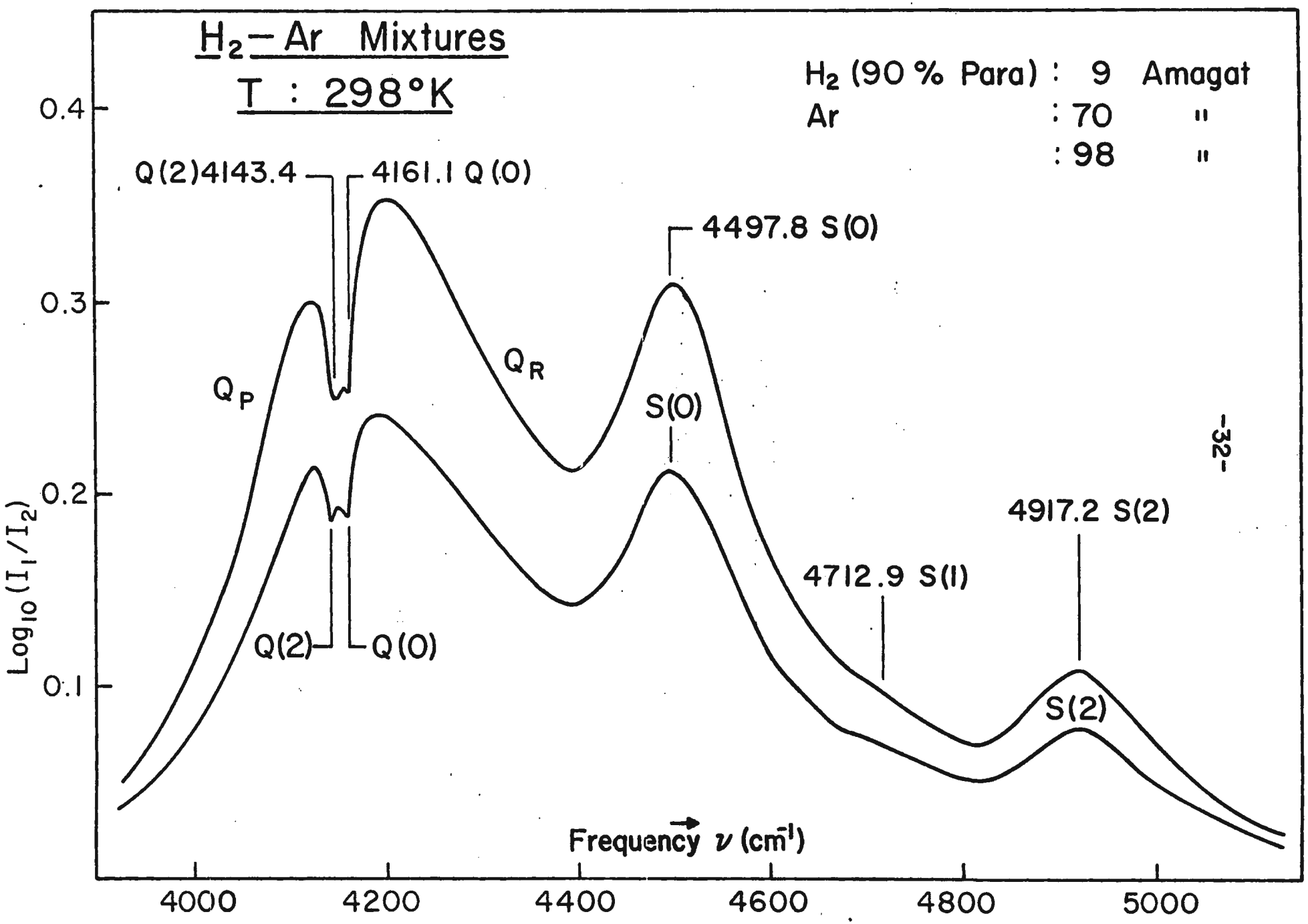
H2 – Ar Mixtures
T : 298°K
H2 (90 % Para) : 9 Amagat
Ar : 70 "
: 98 "
Q(2)4143.4
4161.1 Q(0)
4497.8 S(0)
QP
QR
S(0)
4917.2 S(2)
4712.9 S(1)
Q(2)
Q(0)
S(2)
Log10 (I1/I2)
Frequency ν (cm-1)
0.4
0.3
0.2
0.1
4000
4200
4400
4600
4800
5000

TABLE 7

EXPECTATION OPETATORS OF THE TRIPLET STATE.

PRESSURE atm.	0.	6.54 10^{-2}	3.62 10^{-1}	3.42	2.64 10^{1}	4.11 10^{2}	2.41 10^{3}	1.13 10^{4}	4.17 10^{4}	1.32 10^{5}	2.20 10^{6}
$< 1/r_{12} >$	0.4805	0.4804	0.4805	0.4805	0.4806	0.4805	0.4791	0.4750	0.4658	0.4526	0.4130
$< \eta^2 >$	0.4573	0.4573	0.4573	0.4573	0.4574	0.4575	0.4576	0.4578	0.4585	0.4596	0.4652
$< \eta^4 >$	0.3032	0.3033	0.3032	0.3033	0.3033	0.3034	0.3034	0.3035	0.3039	0.3046	0.3089
$< \xi >$	2.2029	2.2014	2.2006	2.1978	2.1934	2.1738	2.1393	2.0820	1.9949	1.9022	1.7189
$< \xi^2 >$	5.7185	5.7079	5.7022	5.6821	5.6498	5.5121	5.2919	4.9564	4.4895	4.0308	3.2154
$< \xi^3 >$	17.506	17.445	17.409	17.385	17.084	16.267	15.075	13.424	11.342	9.477	6.538
$< \xi^4 >$	62.625	62.275	62.054	61.292	60.055	55.224	48.824	40.830	31.793	24.482	14.364
$< z^2 >$	1.3790	1.3785	1.3772	1.3745	1.3705	1.3551	1.3442	1.3460	1.3778	1.4431	1.7096
$< z^4 >$	5.3176	5.3041	5.2860	5.2374	5.1602	4.8762	4.5992	4.3968	4.3732	4.5808	5.8967
$< r^2 >$	2.6124	2.6109	2.6084	2.6024	2.5936	2.5584	2.5272	2.5111	2.5356	2.6091	2.9428
$< r^4 >$	14.351	14.488	14.437	14.293	14.066	13.213	12.367	11.662	11.339	11.549	13.771
$< r_a >$	1.5651	1.5651	1.5647	1.5640	1.5631	1.5597	1.5605	1.5703	1.5987	1.6446	1.8010
$< r_a^2 >$	3.1171	3.1163	3.1140	3.1088	3.1014	3.0733	3.0593	3.0800	3.1778	3.3567	4.0407
$< r_a^3 >$	7.3880	7.3819	7.3703	7.3419	7.2990	7.1378	7.0186	7.0155	7.2829	7.8594	10.340
$< r_a^4 >$	20.207	20.170	20.115	19.969	19.742	18.903	18.201	17.905	18.548	20.324	28.946

kinetic energies of the colliding pairs of molecules in the absorption process. In collision-induced absorption, the individual quadrupolar components of the band were found to have a Boltzmann-modified dispersion line-shape which can be represented by the following equations:

(3-1) $$\tilde{\alpha}^{-} = \tilde{\alpha}^{+} \exp(-hc\nu_{tr}/kT),$$

(3-2) $$\tilde{\alpha}^{+} = \tilde{\alpha}^{0}/(1 + (\nu - \nu_m)^2/\delta^2), \nu \geq \nu_m.$$

Here, $\tilde{\alpha}^{-}$ and $\tilde{\alpha}^{+}$ (where $\tilde{\alpha} = (1/\nu)\alpha$; note that α's used here represent enhancement absorption coefficients (α_{en})) are absorption coefficients at frequencies $\nu_m - \nu_{tr}$ and $\nu_m + \nu_{tr}$ in the low- and high- frequency wing, respectively; ν_m is the (central) molecular frequency of the line, ν_{tr} is a continuum of frequencies corresponding to the relative translational energy of the colliding pairs of molecules, $\tilde{\alpha}^{0}$ is the peak absorption intensity at $\nu = \nu_m$ and δ is the half-width of the line at half intensity. Figure 10 illustrates the shape of a Boltzmann-modified dispersion line.

According to Van Kranendonk's theory (1958), the expressions for the relative line strengths of the quadrupolar components for the fundamental absorption band in a binary mixture, where the perturbing gas is monatomic (zero quadrupole moment), are as follows:

(3-3) $$\tilde{\alpha}_{1_b}(O(J)) : (Q_1'(J, J-2))^2 P(J) L_2(J, J-2),$$

(3-4) $$\tilde{\alpha}_{1_b}(Q_Q(J)) : (Q_1'(J, J))^2 P(J) L_2(J, J),$$

(3-5) $$\tilde{\alpha}_{1_b}(S(J)) : (Q_1'(J, J+2))^2 P(J) L_2(J, J+2),$$

where $Q_1'(J, J')$ are the first derivatives of the quadrupole moment of the absorbing gas; $P(J)$ are normalized Boltzmann factors, and $L_2(J, J')$ are Racah coefficients. The condition of normalization of $P(J)$ satisfies the relation

$$\sum_{J=0}^{\infty} (2J + 1) P(J) = 1 .$$

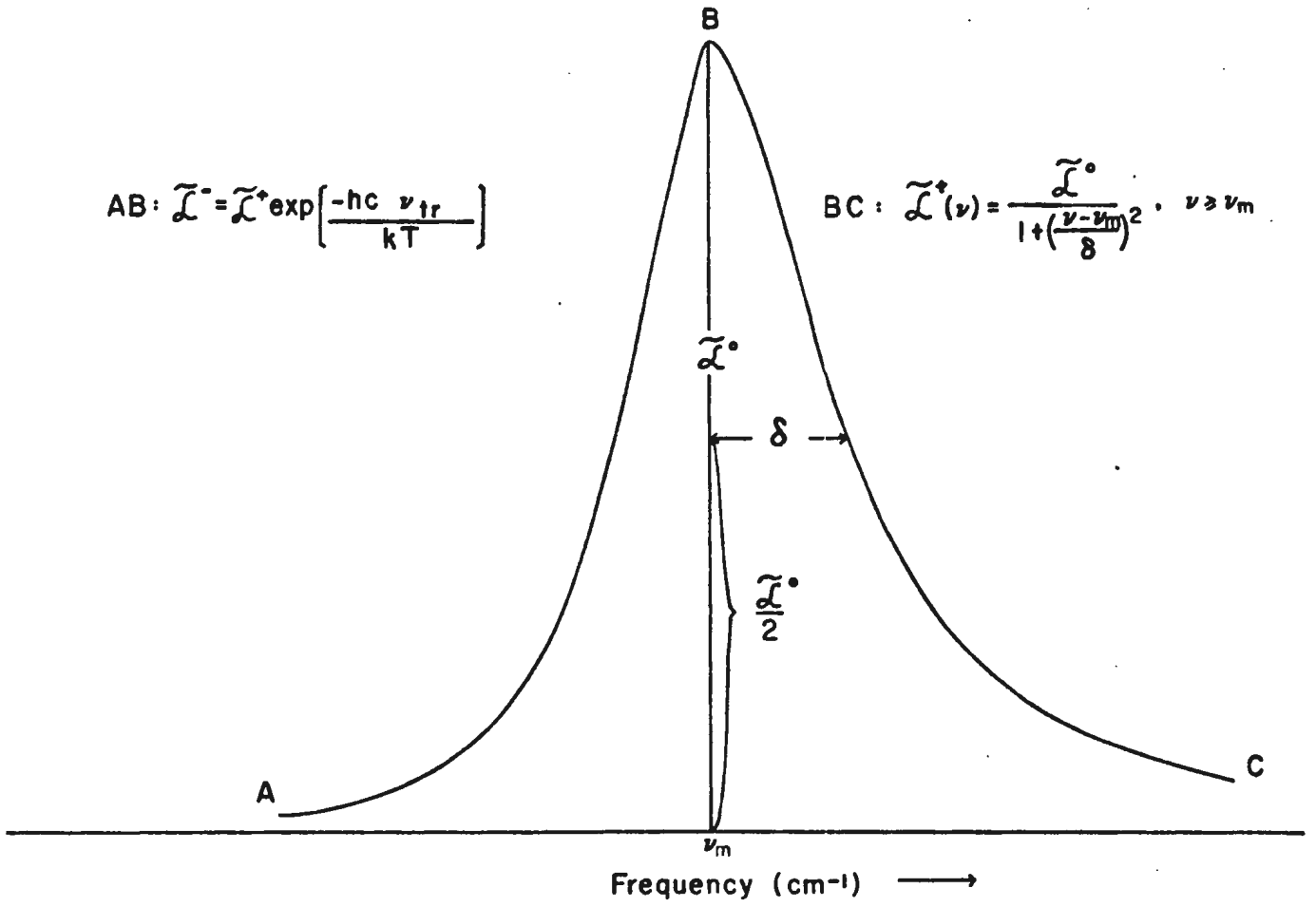

Fig.10. Boltzmann-modified dispersion line form.

Theoretical calculations by the method of adiabatic approximation by Karl and Poll (1967) have shown that $Q_i(J, J')$ of H_2 which are proportional to the matrix elements of its quadrupole moment $\langle V, J|Q|V + 1, J'\rangle$ are strongly dependent on the initial and final rotational quantum numbers J and J' of a transition. To obtain the relative intensities of the four quadrupolar components in a pH_2 - foreign gas mixture, the values of $Q'(J, J')$ were calculated from the matrix elements of the quadrupole moment taken from Birnbaum and Poll (1969) (see Chapter 4). The relative intensities of the quadrupolar single transition components O(2), $Q_Q(2)$ (note $Q_Q(0)$ does not occur in the present cases since the single transition $J = 0 \nrightarrow J' = 0$ is forbidden), S(0), and S(2) of the fundamental band of parahydrogen at room temperature were then calculated by using expressions (3-3) to (3-5) and are listed in Table I.

3.3 Analysis of the Enhancement Absorption Profiles of pH_2 - Xe, pH_2 - Kr, and pH_2 - Ar.

The analysis of the enhancement absorption profiles was carried out by means of a program written for IBM 360/40 computer (see Appendix II). In the analysis, the quadrupolar lines of the band are assumed to have a Boltzmann-modified dispersion line-shape given by eqs. (3-1) and (3-2). The peak intensities of O(2), $Q_Q(2)$, S(0), and S(2) were expressed in terms of the intensity of the most intense line S(0) (see Table I). In the computer program, the value of the half-width δ, assumed to be the same for all quadrupolar components of a hydrogen-foreign gas mixture, as well as the value of $\tilde{\alpha}^0$, the peak intensity of the S(0) component, were left as adjustable parameters; the molecular frequencies ν_m of these components could also be varied easily. Since we used 90% parahydrogen in the

TABLE I

Relative intensities of the quadrupolar single transitions of the fundamental band of parahydrogen at 298^0K

Transition	Frequency (cm^{-1})	$\langle 0J\|Q\|1J'\rangle$ †	Relative intensity
O(2)	3806.7	0.09764	0.278
Q(2)	4143.4	0.08815	0.322
{Q(0)}*	4161.1	0.08793	0.000
S(0)	4497.8	0.07835	1.000
S(2)	4917.2	0.06586	0.325

*Quadrupolar Q(0) line does not occur as a single transition.

†Birnbaum and Poll(1969)

experiments, there is a small contribution of S(1) to the intensity of the absorption profiles. The S(3) line (frequency 5109.0 cm^{-1} for a free molecule; peak intensity 7% that of S(1) at room temperature) is too weak to appear. For the present absorption profiles, the spectral intervals, from 4850 to 5100 cm^{-1} in Figs. 7 and 8 and from 4900 to 5100 cm^{-1} in Fig. 9, are free from the S(1) line. When the frequencies of the quadrupolar components for pH_2 - Xe were unshifted from those of the free molecule, a satisfactory fit to the experimental profile by the calculated profile (using the criterion described below) could not be obtained as can be seen in Fig. 11. The same was found true for the profiles of pH_2 - Kr mixtures. The values of ν_m were then varied in small steps until a best fit to the experimental profile was obtained by the calculated profile; the best fit was judged from the criterion that the sum of the squares of the differences between the calculated and observed intensities at equally spaced frequency intervals over the desired spectral region be a minimum. In this fit, the shift of the quadrupolar components was assumed to be the same for a given binary mixture. The examples of the results of such an analysis for the induced fundamental band of parahydrogen in pH_2 - Xe and pH_2 - Kr mixtures are shown in Figs. 12 and 13, respectively. In both figures, the fit in the interval 4850 to 5100 cm^{-1} is extremely good. In the analysis of the profiles obtained with parahydrogen-argon mixtures, it was not found necessary to shift the quadrupolar components to obtain the best fit. An example of the results of the analysis of the band in pH_2 - Ar mixtures is shown in Fig. 14, where the fit in the interval 4900 to 5100 cm^{-1} is also very good. The results of profile analysis for all the three parahydrogen-foreign gas mixtures are summarized in Table II.

Fig.11. Analysis of the enhancement absorption profile of the H_2 fundamental band in a pH_2-Xe mixture with no shift of the individual components of the band.

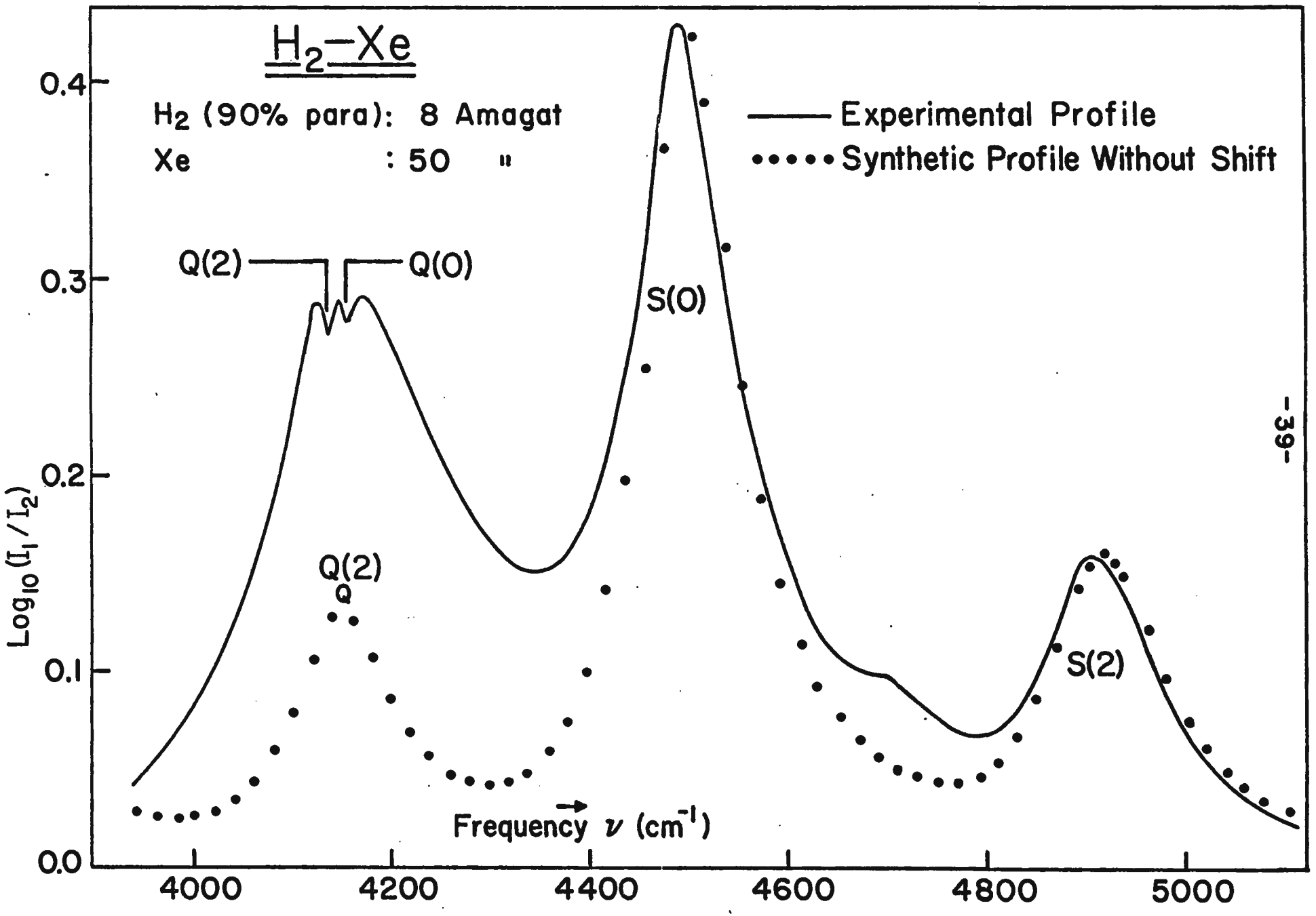
H2–Xe
H2 (90% para): 8 Amagat
Xe : 50 "
Experimental Profile
Synthetic Profile Without Shift
Q(2)
Q(0)
S(0)
Q(2)
S(2)
Log10 (I1 / I2)
Frequency ν (cm-1)
0.0
0.1
0.2
0.3
0.4
4000
4200
4400
4600
4800
5000

Fig.12. The enhancement absorption profile of the H_2 fundamental band in a binary mixture of hydrogen (90% para) and xenon at 298^0K. The solid curve (a) is the experimental profile; the dashed curves represent the individual quadrupolar components O(2), $Q_Q(2)$, S(0), and S(2), and the dots (b) represent the quadrupolar profile which is the summation of these components; the dot-dashed curve (c) is the overlap profile obtained by subtracting (b) from (a) in the region 3900 to 4500 cm^{-1}.

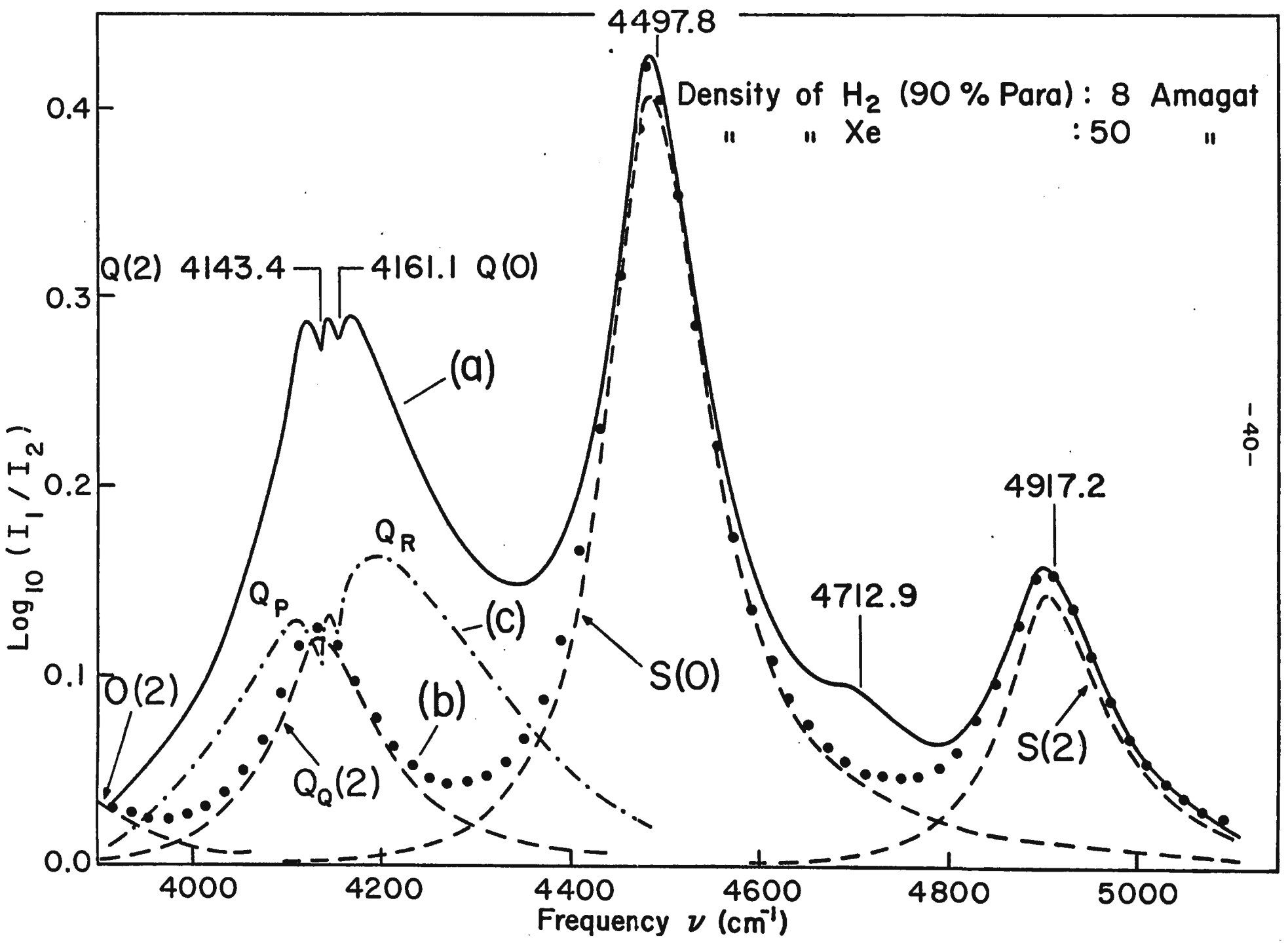
4497.8
Density of H_2 (90 % Para) : 8 Amagat
" " Xe : 50 "
Q(2) 4143.4
4161.1 Q(0)
(a)
4917.2
4712.9
Q_R
Q_P
(c)
S(0)
O(2)
(b)
S(2)
$Q_Q(2)$
$\log_{10}(I_1/I_2)$
0.0
0.1
0.2
0.3
0.4
4000
4200
4400
4600
4800
5000
Frequency ν (cm^{-1})
-40-

Fig.13. The enhancement absorption profile of the H_2 fundamental band in a binary mixture of hydrogen (90% para) and krypton at 298^0K. The solid curve (a) is the experimental profile; the dashed curves represent the individual quadrupolar components O(2), $Q_Q(2)$, S(0), and S(2), and the dots (b) represent the quadrupolar profile which is the summation of these components; the dot-dashed curve (c) is the overlap profile obtained by subtracting (b) from (a) in the region 3900 to 4500 cm^{-1}.

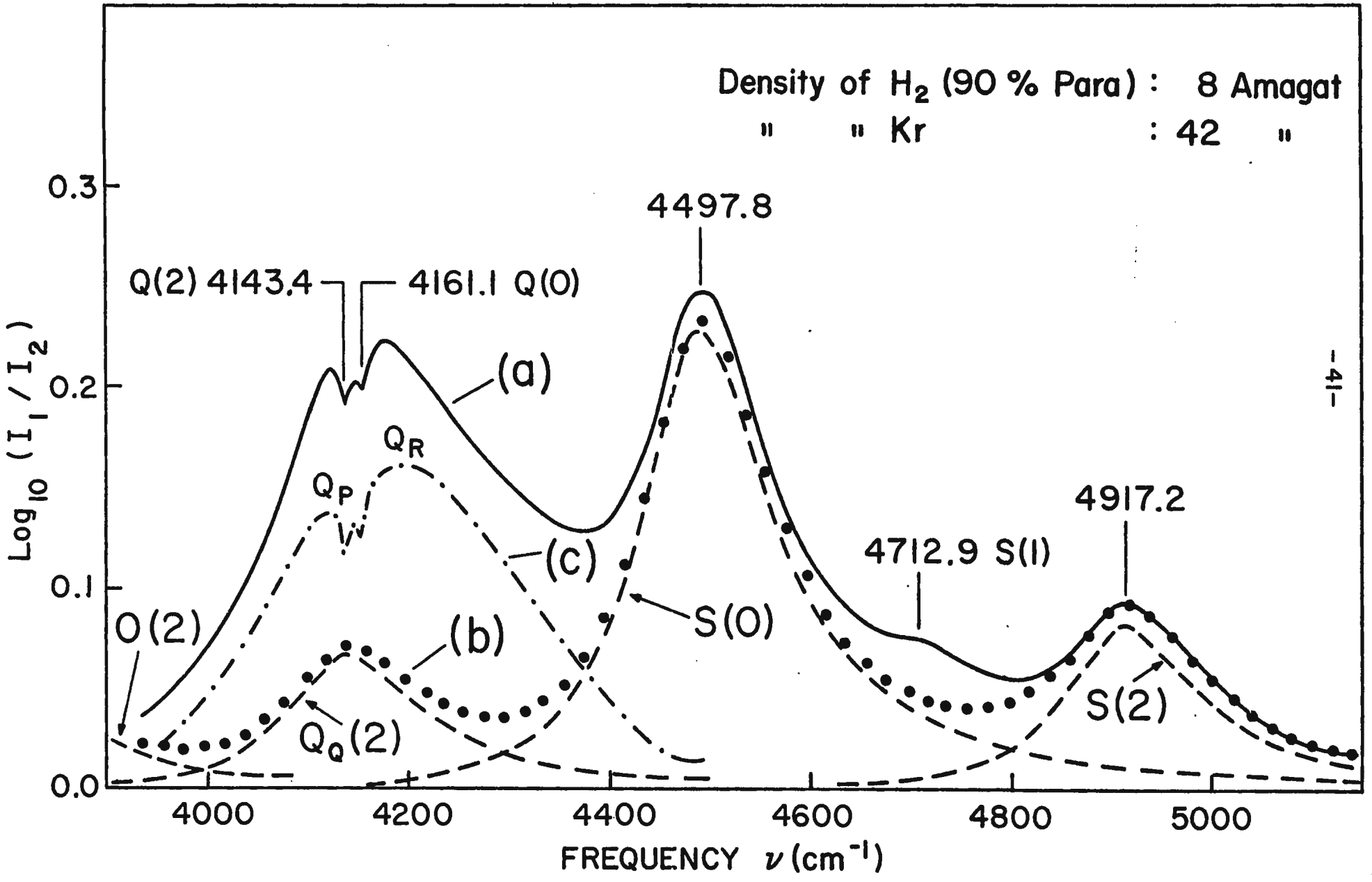
Density of H_2 (90 % Para) : 8 Amagat
" " Kr : 42 "
4497.8
Q(2) 4143.4
4161.1 Q(0)
(a)
Q_R
Q_P
(c)
4917.2
4712.9 S(1)
O(2)
(b)
S(0)
$Q_Q(2)$
S(2)
0.3
0.2
0.1
0.0
$\mathrm{Log}_{10}(I_1/I_2)$
4000
4200
4400
4600
4800
5000
FREQUENCY ν (cm^{-1})

Fig.14. The enhancement absorption profile of the H_2 fundamental band in a binary mixture of hydrogen (90% para) and argon at 298^0K. The solid curve (a) is the experimental profile; the dashed curves represent the individual quadrupolar components O(2), $Q_Q(2)$, S(0), and S(2), and the dots (b) represent the quadrupolar profile which is the summation of these components; the dot-dashed curve (c) is the overlap profile obtained by subtracting (b) from (a) in the region 3900 to 4500 cm^{-1}.

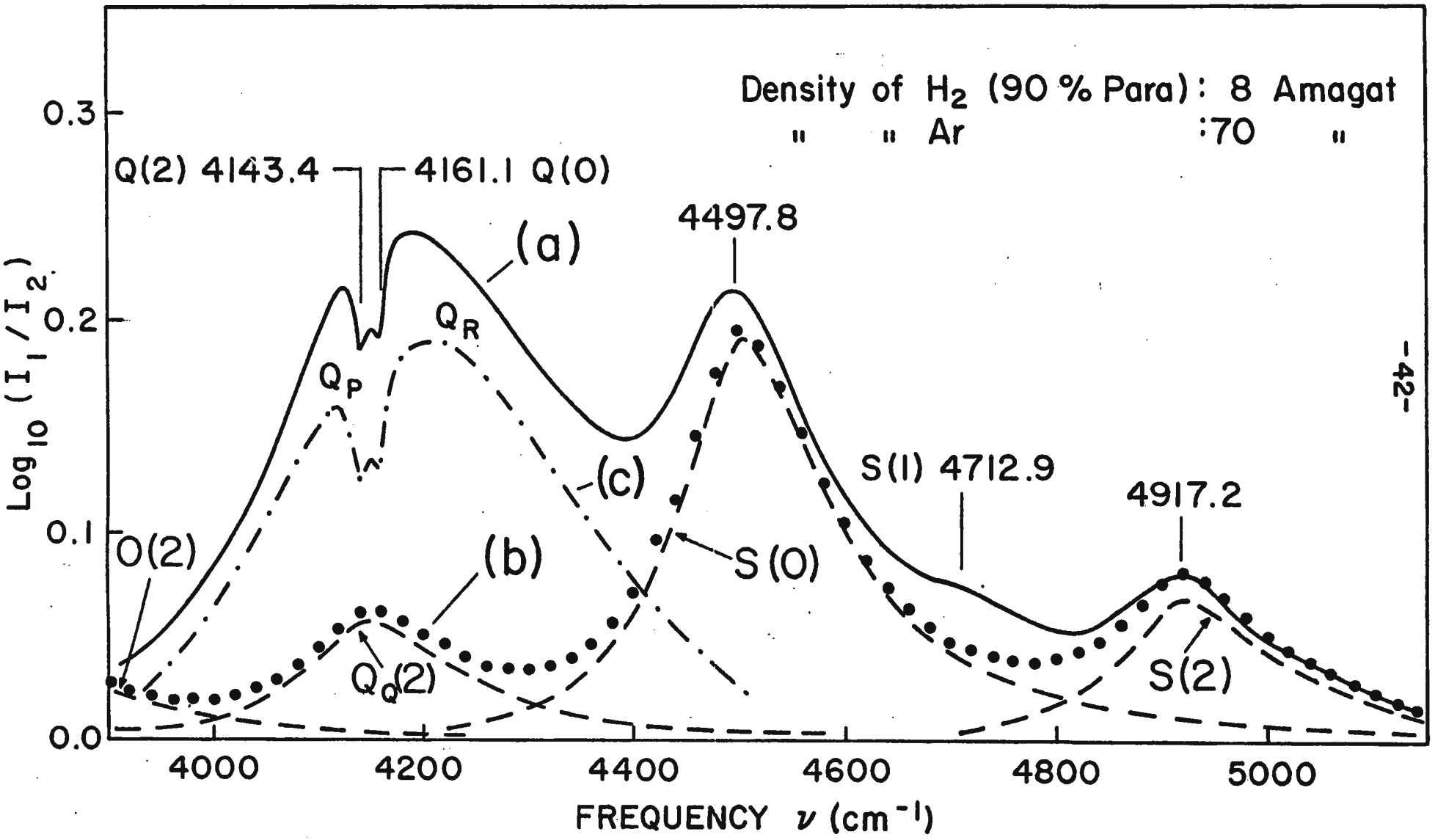
Density of H_2 (90 % Para) : 8 Amagat
" " Ar : 70 "
Q(2) 4143.4
4161.1 Q(0)
4497.8
(a)
Q_R
Q_P
(c)
S(1) 4712.9
4917.2
O(2)
(b)
S(0)
$Q_Q(2)$
S(2)
0.3
0.2
0.1
0.0
$\log_{10}(I_1/I_2)$
4000
4200
4400
4600
4800
5000
FREQUENCY ν (cm^{-1})

TABLE II

Results of the analysis of the profiles obtained with binary mixtures of parahydrogen with Xe, Kr, and Ar at 298^0K

Mixture	Number of profiles analyzed	Frequency shift* of the quadrupole components (cm^{-1})	δ (cm^{-1})
pH_2-Xe	10	9 ± 1	78 ± 2
pH_2-Kr	9	6 ± 1	92 ± 3
pH_2-Ar	8	0 ± 1	102 ± 3

*The shift is toward lower frequency (red shift).

The overlap profile was obtained by subtracting the synthetic quadrupolar profile of a parahydrogen-foreign gas mixture from the corresponding experimental profile. Typical overlap profiles obtained for binary mixtures of parahydrogen with xenon, krypton and argon are also shown in Figs. 12, 13 and 14, respectively. It must be pointed out that these overlap profiles include a small contribution of the quadrupolar component $Q_Q(1)$ (frequency 4155.2 cm^{-1}) (because of 10% orthohydrogen present as impurity). Because of this, we did not attempt to analyze these overlap profiles in parahydrogen-foreign gas mixtures. It is interesting to note that the overlap profile of pH_2 - Xe (Fig. 12) has also its Q_R peak more intense than the Q_P peak. From this we can conclude that the apparent anomaly of intensity of the Q_P and Q_R peaks in the experimental profiles of pH_2 - Xe is due partly to a shift (9 ± 1 cm^{-1}) of the quadrupolar component $Q_Q(2)$ toward lower frequency and partly to its large relative intensity with respect to the Q branch. The shifts of the quadrupolar components of pH_2 - Xe and pH_2 - Kr, quoted in this chapter are found to be independent of density within the range of pressures used in the present experiments. A significant consequence of the occurrence of the dips exactly at Q(0) and Q(2) Raman frequencies in the three mixtures studied above (Figs. 7 to 9 and 12 to 14) is that there is no shift in the overlap components of the Q branch in the collision-induced fundamental band of parahydrogen at room temperature.

3.4 Analysis of the Profiles for the Enhancement of Absorption for nH_2-Xe, nH_2-Kr, and nH_2-Ar

(a) Separation of quadrupolar and overlap parts by the method of profile analysis

Representative experimental profiles for the enhancement of absorption of the induced fundamental band of H_2 at room temperature in the binary mixtures of normal hydrogen (25% para and 75% ortho) with xenon, krypton, and argon have already been presented in Fig. 2 in chapter 1. In this section we present the analysis of the enhancement absorption profiles of the band obtained in these three binary mixtures. The method of analysis is similar to the one used for the profiles of parahydrogen-foreign gas mixtures as described in sections 3.2 and 3.3. The induced fundamental band of normal H_2 at room temperature consists of nine quadrupolar components, O(3), O(2), $Q_Q(J)$ for J = 1 to 3, and S(J) for J = 0 to 3, and four overlap components $Q_{overlap}(J)$, for J = 0 to 3. The Boltzmann-modified dispersion line shape given by eqs. (3-1) and (3-2) was assumed for all the quadrupolar components. Their relative intensities were calculated by using expressions (3-3) and (3-5) and were then expressed in terms of the most intense line S(1). These are listed in Table III. To obtain the best fit of the quadrupolar synthetic profile of nH_2-Xe or nH_2-Kr to the corresponding experimental profile in the S branch region, which is free from the overlap contribution, it was found necessary to shift the molecular frequencies ν_m of the quadrupolar components toward

TABLE III

Relative intensities of the quadrupolar single transitions of the fundamental band of normal hydrogen at 298^0K

Transition	Frequency (cm^{-1})	$\langle 0J\|Q\|1J'\rangle$†	Relative intensity
O(3)	3568.2	0.10410	0.119
O(2)	3806.7	0.09764	0.108
Q(3)	4125.8	0.08836	0.088
Q(2)	4143.4	0.08815	0.125
Q(1)	4155.2	0.08800	0.991
{Q(0)}*	4161.1	0.08793	0.000
S(0)	4497.8	0.07835	0.388
S(1)	4712.9	0.07206	1.000
S(2)	4917.2	0.06586	0.126
S(3)	5109.0	0.05974	0.073

*Quadrupolar Q(0) line does not occur as a single transition

†Birnbaum and Poll(1969)

lower frequency from those of the free molecule. However, for the enhancement absorption profiles of nH_2-Ar obtained in the present work, no shift of the quadrupolar components was found necessary to obtain a good fit. Examples of the results of the profile analysis for nH_2-Xe, nH_2-Kr, and nH_2-Ar are shown in Figs. 15, 16, and 17, respectively. In these figures $\log_{10}(I_1/I_2)$ (= $(\ell/\ln 10)\ \nu\tilde{a}_{en}(\nu)$) is plotted against frequency. The nine quadrupolar components of the bands are shown separately. The fit of the synthetic quadrupolar profiles to the experimental profiles is good in regions 4600 - 5300 cm^{-1} for nH_2-Xe and nH_2-Kr, and 4600 - 5300 cm^{-1} for nH_2-Ar. The shifts of the quadrupolar components and their characteristic half-widths for these mixtures obtained from the profile analysis are summarized in Table IV. The frequency shifts and the characteristic half-widths obtained from the analysis of the profiles of nH_2-foreign gas mixtures are in good agreement with those of the corresponding pH_2-foreign gas mixtures.

The overlap absorption profiles of the band for nH_2-Xe, nH_2-Kr, and nH_2-Ar were obtained by subtracting the synthetic quadrupolar profiles from the corresponding experimental profiles (see Figs. 15 to 17). In section 3.3, the overlap profiles obtained by a similar method for the pH_2-foreign gas mixtures included a small contribution of the $Q_0(1)$ quadrupolar component because of 10% ortho-hydrogen present as an impurity. However, in the present case, the overlap profiles of nH_2-foreign gas mixtures consist entirely of the overlap components $Q_{overlap}(J)$ for J = 0 to 3. The dip between the

Fig.15. The enhancement absorption profile of the hydrogen fundamental band in a binary mixture of nH_2 and Xe. The solid curve is the experimental profile; the dashed curves represent the individual quadrupolar components, and the dots represent the quadrupolar profile which is the summation of these components; the dot-dashed curve is the overlap profile obtained by subtracting the synthetic quadrupolar profile from the experimental profile in the region 3900 to 4600 cm^{-1}.

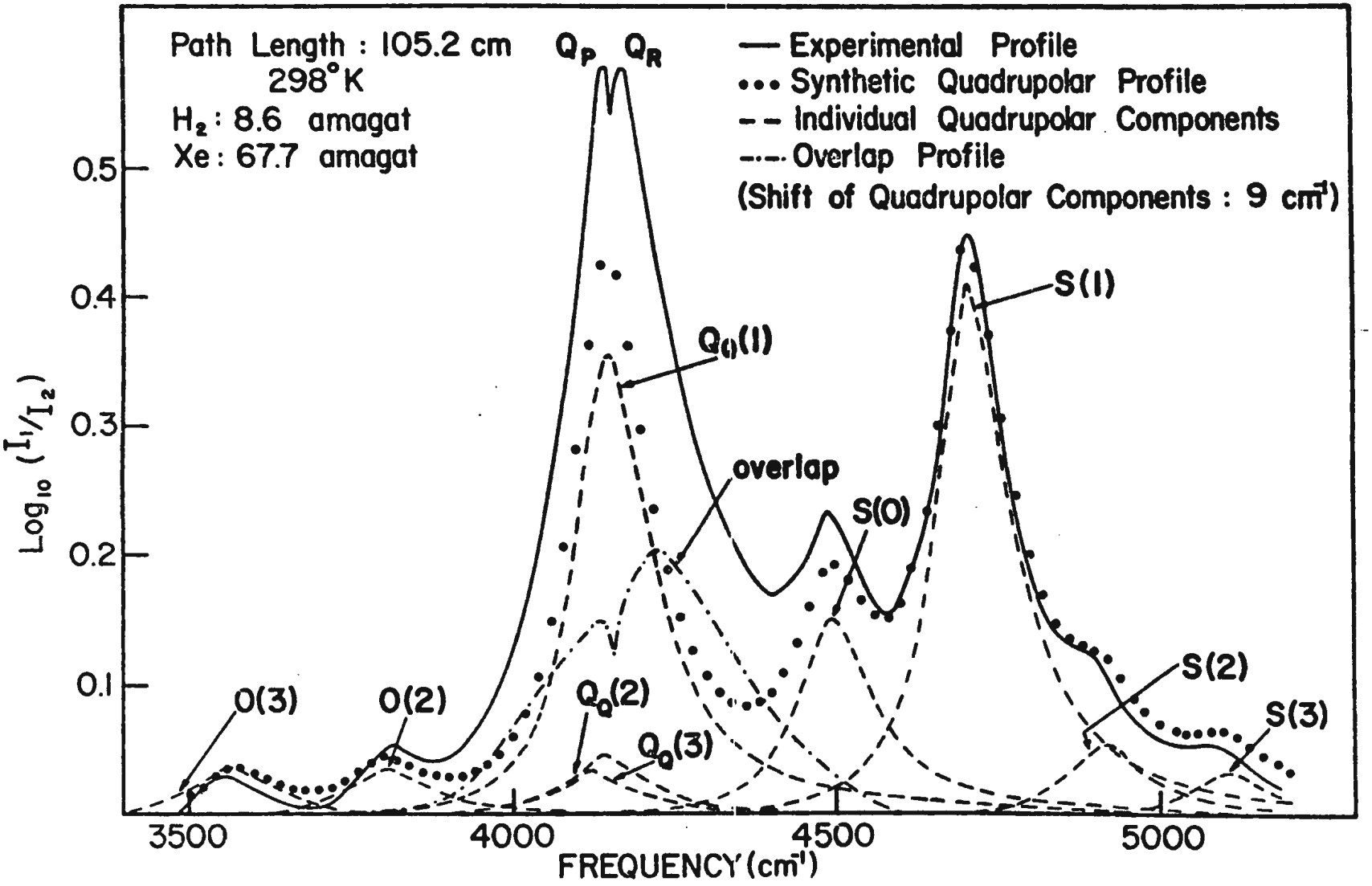
Path Length : 105.2 cm
298°K
H₂ : 8.6 amagat
Xe : 67.7 amagat
Q_P Q_R
— Experimental Profile
••• Synthetic Quadrupolar Profile
– – Individual Quadrupolar Components
–·– Overlap Profile
(Shift of Quadrupolar Components : 9 cm⁻¹)
S(1)
Q₀(1)
overlap
S(0)
S(2)
S(3)
O(3)
O(2)
Q₀(2)
Q₀(3)
0.5
0.4
0.3
0.2
0.1
Log₁₀ (I₁/I₂)
3500
4000
4500
5000
FREQUENCY (cm⁻¹)

Fig.16. The enhancement absorption profile of the H_2 fundamental band in a binary mixture of nH_2 and Kr. The solid curve is the experimental profile; the dashed curves represent the individual quadrupolar components, and the dots represent the quadrupolar profile which is the summation of these components; the dot-dashed curve is the overlap profile obtained by subtracting the synthetic quadrupolar profile from the experimental profile in the region 3900 to 4650 cm^{-1}.

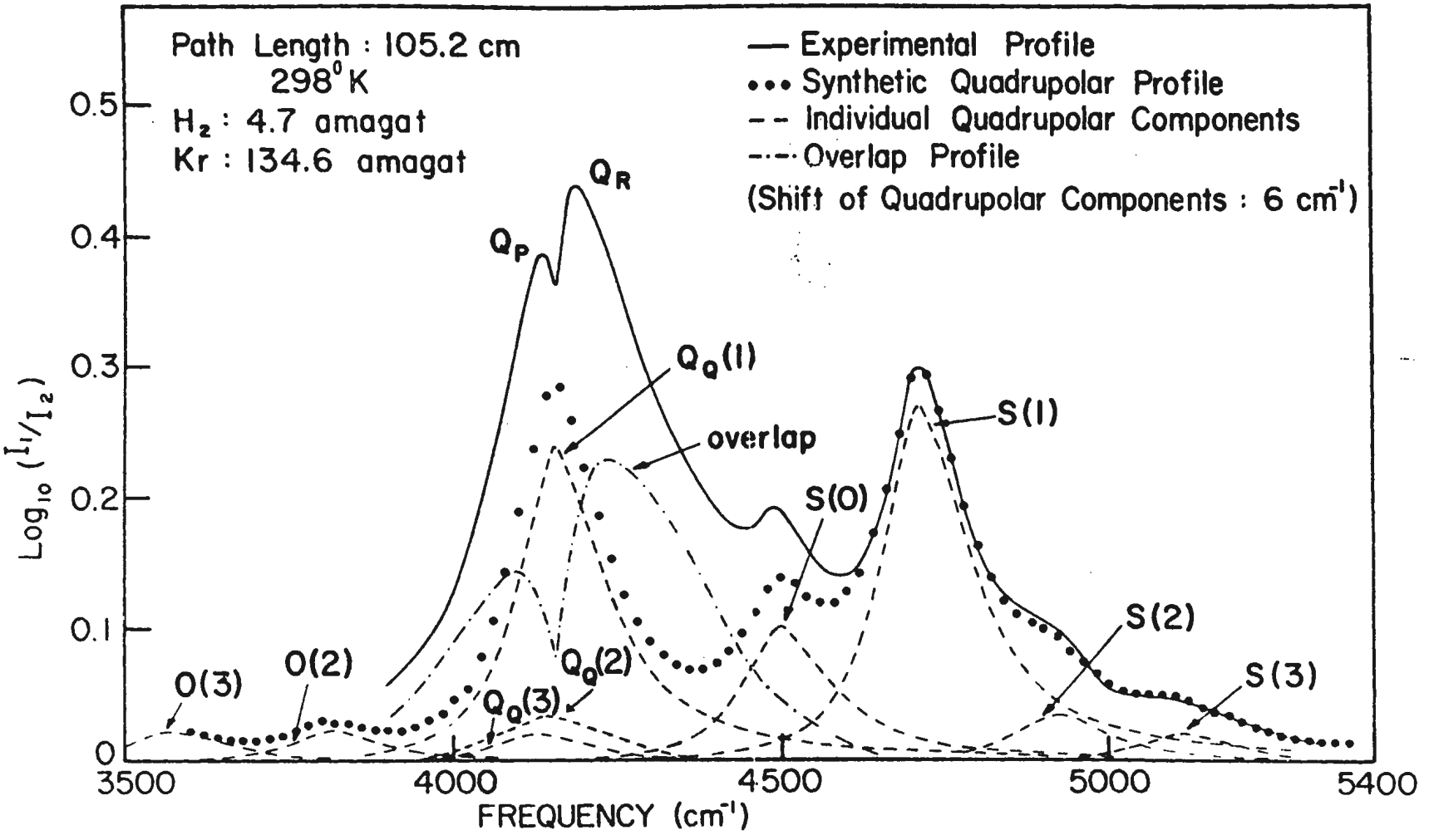
Path Length : 105.2 cm
298°K
H_2 : 4.7 amagat
Kr : 134.6 amagat
— Experimental Profile
••• Synthetic Quadrupolar Profile
-- Individual Quadrupolar Components
-·-· Overlap Profile
(Shift of Quadrupolar Components : 6 cm⁻¹)
Q_R
Q_P
$Q_Q(1)$
overlap
S(0)
S(1)
S(2)
S(3)
O(3)
O(2)
$Q_Q(2)$
$Q_Q(3)$
$\log_{10}(I_1/I_2)$
0.5
0.4
0.3
0.2
0.1
0
3500
4000
4500
5000
5400
FREQUENCY (cm⁻¹)

Fig.17. The enhancement absorption profile of the H_2 fundamental band in a binary mixture of nH_2 and Ar. The solid curve is the experimental profile; the dashed curves represent the individual quadrupolar components, and the dots represent the quadrupolar profile which is the summation of these components; the dot-dashed curve is the overlap profile obtained by subtracting the synthetic quadrupolar profile from the experimental profile in the region 3900 to 4650 cm^{-1}.

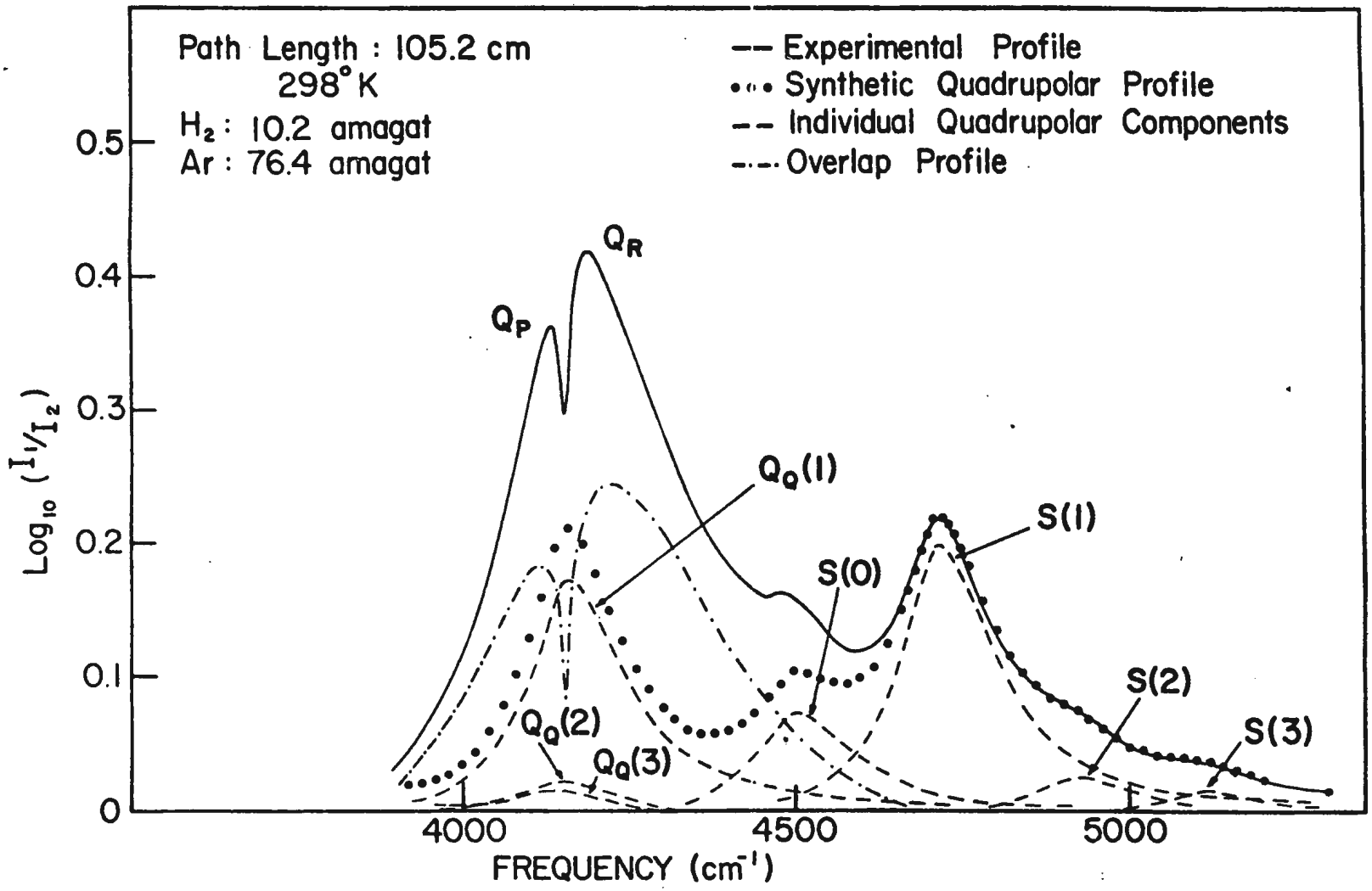
Path Length : 105.2 cm
298° K
H₂ : 10.2 amagat
Ar : 76.4 amagat
— Experimental Profile
••• Synthetic Quadrupolar Profile
– – Individual Quadrupolar Components
–·–· Overlap Profile
Log₁₀ (I₁/I₂)
0.5
0.4
0.3
0.2
0.1
0
Q_R
Q_P
Q_Q(1)
S(1)
S(0)
S(2)
S(3)
Q_Q(2)
Q_Q(3)
4000
4500
5000
FREQUENCY (cm⁻¹)

TABLE IV

Results of the analysis of the profiles obtained with binary mixtures of normal hydrogen with Xe, Kr, and Ar at 298 K^0

Mixture	Frequency shift* of the quadrupolar components (cm^{-1})	δ_{quad} (cm^{-1})	Intracollisional width-parameter δ_W (cm^{-1})	Integrated Absorption	
				Quadrupolar part	Overlap part
nH_2-Xe	9 ± 1	79 ± 2	98 ± 4	75%	25%
nH_2-Kr	6 ± 1	91 ± 3	110 ± 4	67%	33%
nH_2-Ar	0 ± 1	101 ± 3	115 ± 4	58%	42%

* The shift is toward lower frequency (red shift).

Q_P and Q_R peaks of the overlap profile in each of Figs. 15, 16, and 17 occurs at the Q(1) Raman frequency (4155.2 cm^{-1}). This observation lends support to the statement made earlier in section 3.3 in connection with the observation of two dips at the positions of Q(0) and Q(2) Raman frequencies in the Q branch of the band in pH_2-foreign gas mixtures, namely, that there is no shift in the overlap components $Q_{overlap}(J)$ in the induced fundamental band of H_2. It is also seen from Fig. 15 that the overlap profile of nH_2-Xe has its Q_R peak more intense than its Q_P peak, just as in the profiles of the band obtained in other binary mixtures. The apparent anomalous intensity distribution of the Q_P and Q_R peaks in the experimental enhancement absorption profile of nH_2-Xe is due partly to a shift (9 ± 1 cm^{-1}) of the quadrupolar components $Q_Q(1)$, $Q_Q(2)$, and $Q_Q(3)$ toward lower frequency and partly to their large relative intensities with respect to the Q branch. The contributions of the quadrupolar and overlap interactions to the intensity of the band for a given binary mixture can be obtained from the areas under the corresponding profiles. These are estimated for nH_2-Xe, nH_2-Kr, and nH_2-Ar from the profile analysis and are given in Table IV. A further discussion of the percentage contributions of the quadrupolar and overlap interactions to the intensity of the band will be given in chapter 4 in which the quadrupolar binary absorption coefficients of the band in nH_2-Xe, nH_2-Kr, and nH_2-Ar were calculated by using molecular constants of the colliding pairs.

(b) Analysis of the overlap profiles of nH_2-Xe, nH_2-Kr, and nH_2-Ar

As pointed out in chapter 1, Van Kranendonk (1968) showed that the dip observed in the Q branch of the collision-induced fundamental band results on account of an interference effect due to the negative correlations existing between the isotropic parts of the dipole moments induced in successive binary collisions. For isotropically-induced overlap transitions of the Q branch, Van Kranendonk derived a line-shape of the form

$$\tilde{\alpha}(\nu) = \tilde{\alpha}^{o}\, D(\nu)\, W(\nu) \quad . \tag{3-6}$$

Here $D(\nu)$ and $W(\nu)$ are, respectively, the Fourier transforms of the intercollisional and intracollisional correlation functions of the induced dipole moment. Levine and Birnbaum (1967) obtained an analytical expression for the intracollisional part of the line-shape for isotropically-induced transitions using a Gaussian form for the variation of the induced dipole moment with intermolecular separation R with a cut off as $R \to 0$. Levine-Birnbaum's intracollisional line-shape for isotropic transitions can be represented as

$$W(\nu-\nu_m) = ((\nu-\nu_m)/\delta_W)^2 K_2((\nu-\nu_m)/\delta_W) \; ; \quad \nu \geq \nu_m \quad , \tag{3-7}$$

where δ_W is the intracollisional half-width and $K_2((\nu-\nu_m)/\delta)$ is a modified Bessel function of the second kind of order two. Mactaggart and Welsh (private communication) very recently used Levine-Birnbaum's line-shape for the intracollisional part for the overlap components of the fundamental band of H_2 and obtained a good fit of the calculated profile to the experimental profile.

In the present analysis of the overlap profiles we used a dispersion type line-shape for the intercollisional part which can be written as

$$D(\nu-\nu_m) = \{1 - 1/(1 + (\nu-\nu_m)^2/\delta_D^2)\} \quad , \tag{3-8}$$

where δ_D is the intercollisional width-parameter. Levine-Birnbaum's line-shape given by eq. (3-7) was used for the intracollisional part. The resulting line-shape used for the analysis of the overlap profiles can be expressed as follows:

$$\tilde{\alpha}^+(\nu-\nu_m) = \tilde{\alpha}^o \{1 - 1/(1 + (\nu-\nu_m)^2/\delta_D^2)\} \; X \tag{3-9}$$

$$((\nu-\nu_m)^2/\delta_W^2)\; K_2((\nu-\nu_m)/\delta_W) \quad , \quad \nu \geq \nu_m \quad ;$$

$$\tilde{\alpha}^- = \tilde{\alpha}^+ \exp(-hc\nu_{tr}/kT) \quad . \tag{3-10}$$

Here $\tilde{\alpha}^o$ is the fictitious peak intensity at the molecular frequency ν_m of the overlap component, δ_D and δ_W are the intercollisional and intracollisional width-parameters, respectively.

For computation of the synthetic overlap profiles, the relative intensities of the overlap components $Q_{overlap}(J)$, which depend on the factors $P(J)$ and $L_o(J,J)$, were calculated and expressed in terms of the most intense overlap component $Q_{overlap}(1)$. A least-squares fit of the calculated profile to the overlap profile derived from the analysis of experimental absorption profiles, as discussed earlier, was then obtained with the help of a program written for the IBM 360/40 computer (see Appendix I). The criterion for the best fit was the same as the one mentioned earlier in this chapter. As can be

Fig.18. Analysis of the overlap profile obtained in Fig.15 in a nH_2-Xe mixture.

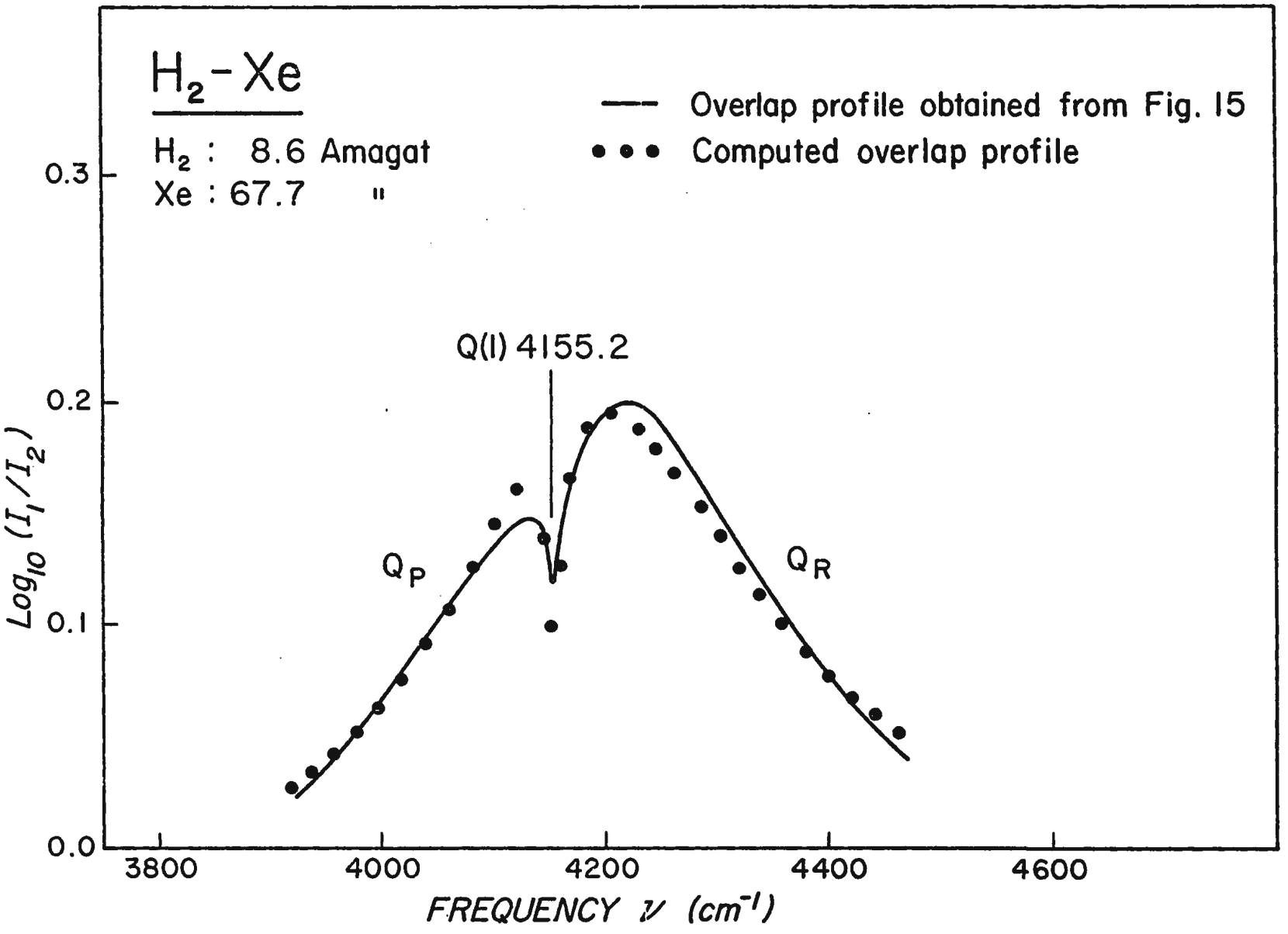
H2 - Xe
H2 : 8.6 Amagat
Xe : 67.7 "
Overlap profile obtained from Fig. 15
Computed overlap profile
Q(1) 4155.2
QP
QR
Log10 (I1/I2)
0.0
0.1
0.2
0.3
3800
4000
4200
4400
4600
FREQUENCY ν (cm-1)

Fig.19. Analysis of the overlap profile obtained in Fig.16 in a nH_2-Kr mixture.

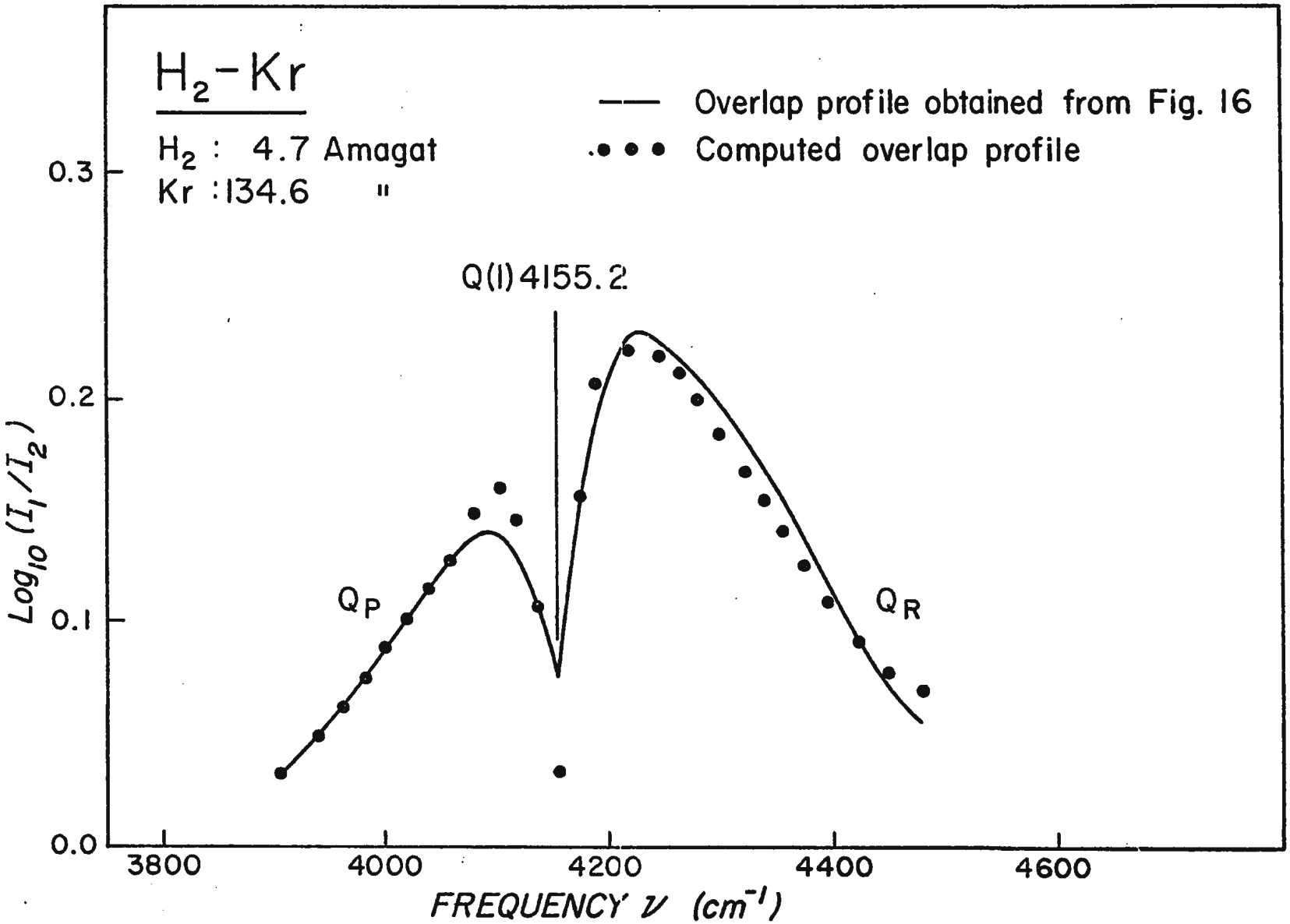
H2-Kr
H2 : 4.7 Amagat
Kr :134.6 "
—— Overlap profile obtained from Fig. 16
• • • Computed overlap profile
Q(1) 4155.2
QP
QR
Log10 (I1/I2)
0.0
0.1
0.2
0.3
3800
4000
4200
4400
4600
FREQUENCY ν (cm-1)

Fig.20. Analysis of the overlap profile obtained in Fig.17 in a nH_2-Ar mixture.

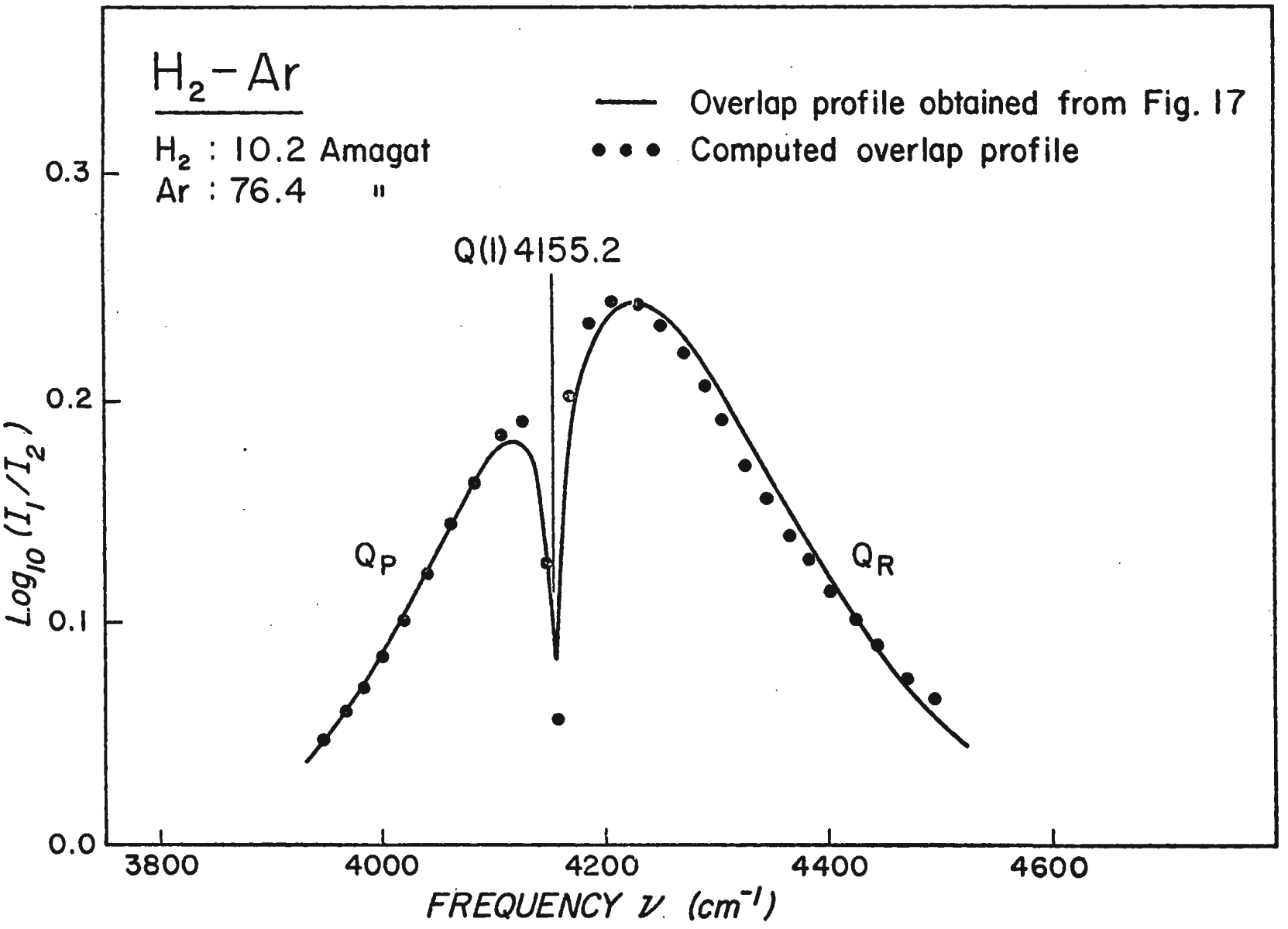
H2 – Ar
H2 : 10.2 Amagat
Ar : 76.4 "
Overlap profile obtained from Fig. 17
Computed overlap profile
Q(1) 4155.2
QP
QR
Log10 (I1/I2)
0.0
0.1
0.2
0.3
3800
4000
4200
4400
4600
FREQUENCY ν (cm-1)

seen from Figs. 18, 19, and 20, the fit of the computed profile to the corresponding overlap profile in each of the binary mixtures, nH_2-Xe, nH_2-Kr, and nH_2-Ar is reasonably good. As expected, it is found that the intercollisional half-width δ_D varies with the density of the perturbing gas whereas the intracollisional half-width δ_W is almost constant within the range of densities used in our experiment. For the overlap profiles shown in Figs. 18, 19, and 20, the intercollisional half-widths are 4, 15, and 10 cm^{-1}, respectively. The intracollisional width-parameters for the three binary mixtures are listed in Table IV.

CHAPTER 4

THE ABSORPTION COEFFICIENTS

In the previous chapter we presented the experimental absorption profiles of the fundamental band of hydrogen in binary mixtures of para-hydrogen as well as normal hydrogen with argon, krypton, and xenon and the analysis of these profiles. Apart from other results, this analysis enabled us to determine the individual contributions of the overlap and quadrupolar intereactions to the intensity of the absorption profiles of the band obtained with normal hydrogen. In principle, using the theory of the exp - 4 model, one can also calculate the quadrupolar parts of the binary absorption coefficients from the known molecular constants of the colliding molecules. In section 4.1 of the present chapter, the absorption coefficients of the band in binary mixtures of normal hydrogen with argon, krypton, and xenon are determined. In section 4.2, the quadrupolar parts are calculated from the molecular constants and the discrepancies obtained are discussed; finally the binary absorption coefficients of the S(0) line obtained from the profile analysis are used to calculate the Lennard - Jones molecular diameter σ for H_2 - Kr and H_2 - Xe pairs.

4.1 Determination of the Absorption Coefficients

The enhancement integrated absorption coefficient of a collision-induced band per unit sample path length, $\int\alpha_{en}(\nu)d\nu$, is expressed in the form

$$\int\alpha_{en}(\nu)d\nu = \alpha_{1_b}\rho_a\rho_b + \alpha_{2_b}\rho_a\rho_b^2 + \ldots \quad (4\text{-}1)$$

Here, $\alpha_{en}(\nu)$ (= $(2.303/\ell)\ \log_{10}\ (I_1(\nu)/I_2(\nu))$, see chapter 2) is the enhancement absorption coefficient at a particular frequency (cm^{-1}); ρ_a

and ρ_b are the partial densities (in units of amagat) of the absorbing and perturbing gases, respectively; α_{1_b} (cm^{-2} amagat $^{-2}$) and α_{2_b} (cm^{-2} amagat $^{-3}$) are the binary and ternary absorption coefficients respectively. In order to make use of the theory, the enhancement absorption coefficients can be represented as

(4-2) $$c\int\alpha_{en}(\nu)d\nu = \tilde{\alpha}_{1_b}\tilde{\rho}_a\tilde{\rho}_b + \tilde{\alpha}_{2_b}\tilde{\rho}_a\tilde{\rho}_b^2 + \ldots .$$

Here c is the speed of light, $\tilde{\alpha}_{en}(\nu)$ ($= \alpha_{en}(\nu)/\nu$) is the enhancement in absorption at a frequency ν with the frequency factor removed $\tilde{\rho}_a$ and $\tilde{\rho}_b$ are the number of molecules per unit volume, of the absorbing and perturbing gases, respectively, and are related to ρ_a and ρ_b by the relations,

(4-3) $$\tilde{\rho}_a = \rho_a n_o \text{ and } \tilde{\rho}_b = \rho_b n_o,$$

n_o being Loschmidt's number (number density of an ideal gas at S.T.P, $2.687 \times 10^{19} cm^{-3}$). The binary and ternary absorption coefficients in (4-2) are related to those in (4-1) by the relations

(4-4) $$\tilde{\alpha}_{1_b} = (c/n_o^2)\ \alpha_{1_b}/\tilde{\nu}\ , \qquad \text{and}$$

$$\tilde{\alpha}_{2_b} = (c/n_o^3)\ \alpha_{2_b}/\tilde{\nu}\ ,$$

where $\tilde{\nu}$ the centre of the band is represented by

(4-5) $$\tilde{\nu} = \int\alpha_{en}(\nu)d\nu\ /\int\nu^{-1}\alpha_{en}(\nu)d\nu.$$

The new binary and ternary absorption coefficients $\tilde{\alpha}_{1_b}$ ($cm^6 s^{-1}$) and $\tilde{\alpha}_{2_b}$ ($cm^9 s^{-1}$) represent the transition probabilities induced in collisions of types a - b and b - a - b respectively.

The integrated absorption coefficients $\int\alpha_{en}(\nu)d\nu$ were obtained by numerically integrating the areas under the enhancement absorption profiles. The partial densities, ρ_a of hydrogen and ρ_b of argon, krypton or xenon used in the present experiments and the corresponding values of $\int\alpha_{en}(\nu)d\nu$

and $(1/\rho_a\rho_b) \int\alpha_{en}(\nu)d\nu$ are presented in Table V. The values of $(1/\rho_a\rho_b) \int\alpha_{en}(\nu)d\nu$ were then plotted against ρ_b as shown in Fig. 21. These plots are found to be straight lines, whose intercepts and slopes give the binary and ternary absorption coefficients, respectively. The values of these coefficients obtained by a least squares straight line fit with the help of IBM 360/40 computer are listed in Table VI. The average values of $\bar{\nu}$ of the band (eq. 4-5) for H_2 - Ar, H_2 - Kr and H_2 - Xe at room temperature are 4385 cm^{-1}, 4390 cm^{-1}, and 4395 cm^{-1}, respectively. The values of $\tilde{\alpha}_{1_b}$ (calculated from eq. 4-4) are also included in Table VI. Finally the values of $\dot{\alpha}_{1_b}$ for H_2 - Ar, H_2 - Kr and H_2 - Xe, obtained by previous researchers are also included in the same table for the purpose of comparison. As can be seen from the table, the binary absorption coefficients for H_2 - Ar, H_2 - Kr and H_2 - Xe mixtures obtained in the present work agree reasonably well with those obtained by previous authors.

4.2 Calculations and Discussion

In the exp - 4 model, the explicit expressions for the binary absorption coefficients of the individual quadrupolar lines of the O, Q, and S branches of an induced fundamental band of a symmetric diatomic gas in a binary mixture with a monatomic perturbing gas (zero quadrupole moment) can be written as

(4-6) $$\tilde{\alpha}_{1_b}[O(J)] = \mu_1^2 \mathcal{J}\, \tilde{\gamma}.P(J).L_2(J, J-2),$$

(4-7) $$\tilde{\alpha}_{1_b}[Q_Q(J)] = \mu_1^2 \mathcal{J}\, \tilde{\gamma}\, .P(J).L_2(J,J),$$

(4-8) $$\tilde{\alpha}_{1_b}[S(J)] = \mu_1^2 \mathcal{J}\, \tilde{\gamma}.P(J).L_2(J, J+2).$$

Here $\mu_1 = (Q_1'\alpha_2/e\sigma^4)$, where Q_1' is the first derivative of the quadrupole moment of the absorbing molecule with respect to internuclear separation,

TABLE V

Enhancement of the integrated absorption coefficients of the fundamental band of H_2 in H_2-Ar, H_2-Kr and H_2-Xe mixtures at 298^{0}K

ρ_{H_2} (amagat)	ρ_b (amagat)	$\int\alpha_{en}(\nu)d\nu$ (cm^{-2})	$(1/\rho_a\rho_b)\int\alpha_{en}(\nu)d\nu$ (10^{-3} cm^{-2} $amagat^{-2}$)
H_2-Ar			
16.6	29.7	2.18	4.42
	41.7	3.12	4.49
	54.9	4.06	4.45
	67.4	5.08	4.53
11.8	7.5	0.38	4.35
	13.7	0.72	4.42
	21.2	1.12	4.47
	30.3	1.59	4.45
	43.6	2.31	4.49
	57.6	3.03	4.46
	70.5	3.77	4.53
10.1	9.5	0.42	4.31
	17.1	0.77	4.45
	23.7	1.06	4.43
	30.6	1.38	4.47
	36.5	1.65	4.49
	43.6	2.00	4.53
	49.4	2.24	4.49

TABLE V (continued)

ρ_{H_2} (amagat)	ρ_b (amagat)	$\int \alpha_{en}(\nu)d\nu$ (cm^{-2})	$(1/\rho_a \rho_b)\int \alpha_{en}(\nu)d\nu$ (10^{-3} cm^{-2} $amagat^{-2}$)
10.1	56.1	2.57	4.54
	62.8	2.83	4.46
	69.1	3.14	4.50
	76.4	3.48	4.51
	83.2	3.78	4.50
	90.5	4.16	4.55
	97.8	4.50	4.56
H_2-Kr			
7.2	7.9	0.45	7.89
	17.1	0.96	7.78
	24.4	1.41	8.01
	32.5	1.86	7.96
	40.2	2.30	7.94
	49.0	2.82	7.99
	56.6	3.19	7.84
	66.4	3.73	7.79
	76.6	4.42	8.01
	85.8	5.02	8.13
5.8	19.2	0.89	8.02
	29.3	1.37	8.03
	40.3	1.87	7.97

TABLE V (continued)

ρ_{H_2} (amagat)	ρ_b (amagat)	$\int\alpha_{en}(\nu)d\nu$ (cm^{-2})	$(1/\rho_a\rho_b)\int\alpha_{en}(\nu)d\nu$ (10^{-3} cm^{-2} $amagat^{-2}$)
5.8	50.5	2.32	7.91
	60.7	2.81	7.94
	74.1	3.44	7.97
	86.9	4.04	7.98
	101.4	4.76	8.06
	114.4	5.31	7.98
4.7	25.5	0.92	7.74
	40.1	1.51	8.06
	54.0	2.02	8.04
	69.4	2.62	8.09
	86.3	3.22	8.00
	103.4	3.86	8.02
	122.4	4.62	8.10
	134.6	5.24	8.08
H_2-Xe			
8.6	16.8	1.70	11.76
	21.8	2.20	11.72
	27.3	2.72	11.56
	33.4	3.28	11.40

Fig.21. Relation between the enhancements in the integrated absorption coefficients of the H_2 fundamental band and the partial densities ρ_a and ρ_b of the binary mixtures nH_2-Ar, nH_2-Kr, and nH_2-Xe.

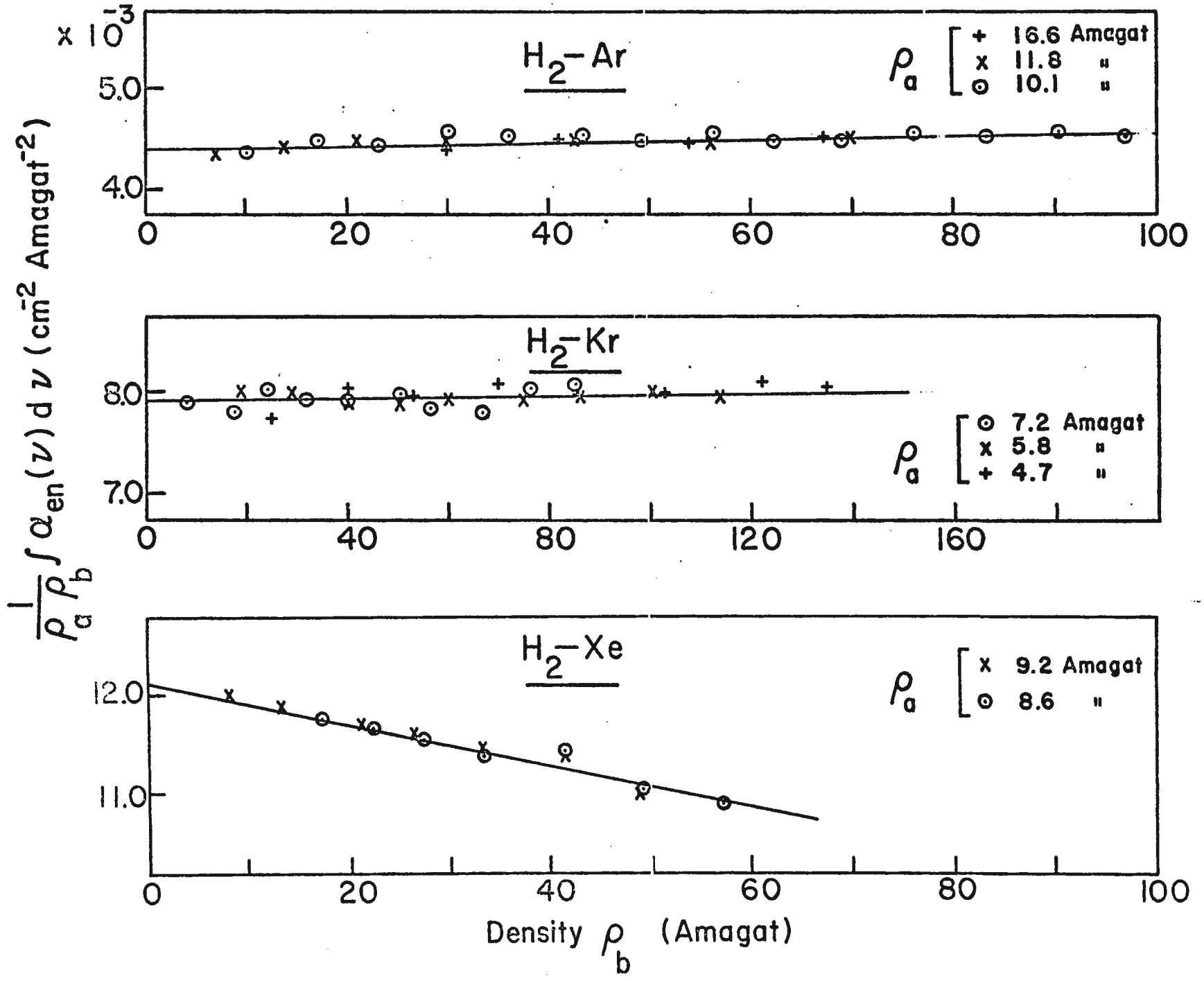
H2–Ar
ρa
+ 16.6 Amagat
x 11.8 "
⊙ 10.1 "
x 10⁻³
5.0
4.0
0
20
40
60
80
100
H2–Kr
ρa
⊙ 7.2 Amagat
x 5.8 "
+ 4.7 "
8.0
7.0
0
40
80
120
160
H2–Xe
ρa
x 9.2 Amagat
⊙ 8.6 "
12.0
11.0
0
20
40
60
80
100
Density ρb (Amagat)
1/ρa ρb ∫ αen(ν) d ν (cm⁻² Amagat⁻²)

TABLE VI

Absorption coefficients of the induced fundamental band of hydrogen in H_2-Ar, H_2-Kr and H_2-Xe mixtures at room temperature

Mixture	Binary absorption coefficient		Ternary absorption coefficient	Reference
	(10^{-3} cm^{-2} $amagat^{-2}$)	(10^{-35} cm^6 s^{-1})	(10^{-6} cm^{-2} $amagat^{-3}$)	
H_2-Ar	4.40 ±.05	4.16	1.7	Present work
	4.5	-	3	Chisholm and Welsh(1954)
	4.1	3.86	3.9	Hare and Welsh(1958)
	4.22	-	-	Hunt(1959)
H_2-Kr	7.91 ±.05	7.46	1.1	Present work
	8.02 ±.01	7.56	0.09	Reddy and Lee(1968)
H_2-Xe	12.11 ±.05	11.45	-19.5	Present work
	11.99 ±.05	11.34	-15.8	Varghese and Reddy(1969)

α_2 is the polarizability of the perturbing molecule, e is the absolute value of the electronic charge and σ is the Lennard - Jones intermolecular separation R for which the intermolecular potential V(R) is zero. $\tilde{\gamma}$ is a constant defined as

(4-9) $$\tilde{\gamma} = (\pi e^2 \sigma^3 / 3 m_0 \nu_0) ,$$

where m_0 and ν_0 are, respectively, the reduced mass and the frequency of vibration of the absorbing molecule. The quantities $L_2(J,J')$ are Racah coefficients and P(J) are the normalized Boltzmann factors for the absorbing molecules; $\mathcal{J}$ is the dimensionless radial distribution integral given by

(4-10) $$\mathcal{J} = 12\pi \int_0^\infty x^{-8} g_0(x) x^2 dx ,$$

where $x = R/\sigma$ and $g_0(x)$ is the low density limit of the pair distribution function. At higher temperatures the classical value $\mathcal{J}_{cl}$ of $\mathcal{J}$ can be calculated by using the pair distribution function

(4-11) $$g_0(x) = \exp(-\Phi(x)/kT),$$

where $\Phi(x)$ is taken as the Lennard - Jones intermolecular potential

(4-12) $$\Phi(x) = 4\varepsilon(x^{-12} - x^{-6}),$$

ε being the depth of the potential. At intermediate temperatures, $g_0(x)$ can be expanded as an asymptotic series in powers of Planck's constant h. The resulting expansion is represented as (Van Kranendonk and Kiss, 1959)

(4-13) $$\mathcal{J} = \mathcal{J}_{cl} - \Lambda^{*2} \mathcal{J}^{(2)} + \Lambda^{*4} \mathcal{J}^{(4)} + \ldots ,$$

where $\mathcal{J}^{(2)}$ and $\mathcal{J}^{(4)}$ are the quantum corrections, and Λ^* $(=(h^2/2m_{00}\varepsilon\sigma^2)^{\frac{1}{2}})$ (m_{00} being the reduced mass of the colliding pair of molecules) is the reduced mean de Broglie wavelength.

As discussed in chapter 3, the calculations of Karl and Poll (1967) and Birnbaum and Poll (1969) have shown that the matrix elements of

the quadrupole moment of H_2, $\langle vJ|Q|v'J'\rangle$ are strongly dependent on v, J, v' and J'. Consequently, Q' of μ_1 in eqs. (4-6) to (4-8) is also a function of J and J' for each of the O, Q_Q, and S branches of the fundamental band of H_2. It is given by the approximate relation

$$Q'(J, J') = (1/r_e(B/\omega)^{1/2}) \langle 0J|Q|1J'\rangle. \qquad (4\text{-}14)$$

The values of Q' for different transitions of the band were derived from those of the matrix elements $\langle 0J|Q|1J'\rangle$ given by Birnbaum and Poll (1969) (see chapter 3) by using eq. (4-14). For H_2, $r_e = 1.40108a_o$, B = 59.3 cm^{-1} ω = 4161 cm^{-1} (Stoicheff 1957). The binary absorption coefficients of the individual quadrupolar transitions were then calculated from eqs. (4-6) to (4-8) and later summed to give the total quadrupolar coefficient. The details of these calculations are summarized below. The molecular parameters used in the calculations are listed in Table VII.

Values of σ and ε/k for hydrogen were taken from Michels, De Graaff, and Ten Seldam (1960) and those for Ar, Kr, and Xe were taken from Hirschfelder, Curtiss, and Bird (1967). For the mixtures, the arithmetic mean $\frac{1}{2}(\sigma_1 + \sigma_2)$ and the geometric mean $(\varepsilon_1\varepsilon_2)^{1/2}/k$ were used. Van Kranendonk and Kiss (1959) have evaluated the values J_{cl}, $J^{(2)}$ and $J^{(4)}$ for a number of reduced temperatures $T^* = T/(\varepsilon/k)$. Using these values, the J values for different mixtures at room temperature ($T = 298^oK$) were calculated with the help of eq. (4-13). The values of $\tilde{\gamma}$ were calculated by using eq. (4-9). The polarizabilities of argon and xenon were taken from Bridge and Buckingham (1964) and that of krypton was taken from Hirschfelder, Curtiss, and Bird (1967). Values of P(J) and $L_2(J, J')$ were calculated as discussed in chapter 3. The calculated binary absorption coefficients of

TABLE VII

Molecular constants for H_2-Ar, H_2-Kr and H_2-Xe mixtures

Mixture	σ (Å)	ϵ/k (°K)	α_2/a_0^3 (for perturber)	T^*	$\tilde{\gamma}$ (10^{-32} cm^6 s^{-1})	Λ^*	$\mathcal{J}$
H_2-Ar	3.232	65.75	11.23	4.53	7.81	0.853	12.09
H_2-Kr	3.260	79.23	16.80	3.76	8.17	0.756	11.93
H_2-Xe	3.530	90.07	27.76	3.31	10.18	0.656	11.91

the individual quadrupolar components and their sum are listed in Table VIII. Finally the overlap parts of the binary absorption coefficients were obtained by subtracting the calculated quadrupolar parts from the corresponding experimental values of $\tilde{\alpha}_{1_b}$. The values of the quadrupolar and the overlap parts for all the three binary mixtures are summarized in Table IX. It is seen that for the binary mixtures H_2 - Ar, H_2 - Kr, and H_2 - Xe, the quadrupolar contributions at room temperature are respectively 32%, 37%, and 46% of the total binary coefficients; however the corresponding values obtained from the profile analysis (see chapter 3, Table IV) are 58%, 67% and 75%, respectively. This striking discrepancy between the calculated and experimental values of the quadrupolar contributions may probably be attributed to the uncertainty in the values of σ for the present binary mixtures (for which the perturbing molecules are much heavier than the absorbing molecule H_2) obtained from the empirical relation, $\sigma_{mix} = \frac{1}{2}(\sigma_1 + \sigma_2)$. This is because σ occurs in the 5th power in the expressions for the quadrupolar binary absorption coefficients (eqs. (4-6) to (4-8)) and a small uncertainty in σ causes a very large error in these absorption coefficients.

We now describe the calculation of the Lennard - Jones intermolecular diameters σ for the H_2 - Kr and H_2 - Xe pairs from the binary absorption coefficients of the S(0) line as obtained from the analysis of the enhancement absorption profiles of the band in binary mixtures of para-hydrogen with Kr and Xe. The binary absorption coefficient of the S(0) line can be written in the following form using eqs. (4-8), (4-9) and (4-14):

TABLE VIII

Quadrupolar parts of binary absorption coefficient of the fundamental band of hydrogen in H_2-Ar, H_2-Kr and H_2-Xe mixtures at room temperature in units of 10^{-35} cm^6 s^{-1}

Mixture	O(3)	O(2)	$Q_Q(1)$	$Q_Q(2)$	$Q_Q(3)$	S(0)	S(1)	S(2)	S(3)	Total
H_2-Ar	0.05	0.05	0.44	0.06	0.04	0.17	0.45	0.06	0.03	1.35
H_2-Kr	0.11	0.10	0.90	0.11	0.08	0.34	0.92	0.12	0.07	2.75
H_2-Xe	0.20	0.19	1.70	0.21	0.15	0.66	1.74	0.22	0.12	5.19

TABLE IX

Binary absorption coefficients and their quadrupolar and overlap components of the induced fundamental band of hydrogen at room temperature

Mixture	Binary absorption coefficient (10^{-35} cm^6 s^{-1})	Quadrupole part* (10^{-35} cm^6 s^{-1})	Overlap part (10^{-35} cm^6 s^{-1})	Percentage	
				Quadrupole	Overlap
H_2-Ar	4.16	1.35	2.81	32	68
H_2-Kr	7.46	2.75	4.71	37	63
H_2-Xe	11.34	5.19	6.15	46	54

*Calculated from Molecular constants using exp -4 model.

(4-15) $$\tilde{\alpha}_{1_b}(S(0)) = (1/\sigma^5)\ (\pi/3m_o\nu_o)\times$$
$$\{(1/r_e(B/\omega)^{\frac{1}{2}}\ \alpha_2)\ \langle 00|Q|1\ 2\rangle\}^2\times$$
$$\mathcal{J}\ .P(0).L_2(0,2).$$

The values of $\tilde{\alpha}_{1_b}$ for S(0) lines of H_2 - Kr and H_2 - Xe were derived from the intercepts of the straight line graphs obtained when $(1/\rho_a\rho_b)\ \int\alpha_{en}(\nu)d\nu$ for the S(0) line was plotted against ρ_b. Here $\int\alpha_{en}(\nu)d\nu$ for the S(0) line was derived from the area of the S(0) line obtained from the analysis of the absorption profiles of pH_2 - Kr and pH_2 - Xe mixtures. The values of σ for H_2 - Kr and H_2 - Xe were then calculated by substituting the numerical values of other quantities in eq. (4-15), and are listed in Table X. It can be seen that the values of σ for both H_2 - Kr and H_2 - Xe pairs thus obtained are considerably smaller than the corresponding values obtained by the empirical relation $\sigma_{mix} = \frac{1}{2}(\sigma_1 + \sigma_2)$.

It must be pointed out here that $\mathcal{J}$ in eq. (4-15) depends on ε, the depth of the Lennard - Jones intermolecular potential of the colliding pairs of molecules (see eqs. (4-10) to (4-11). The values of $\mathcal{J}$ used in the above calculations were obtained by using the values of ε for the mixtures as obtained from the empirical relation $\varepsilon = (\varepsilon_1\varepsilon_2)^{\frac{1}{2}}$. It has been found by direct calculation of $\mathcal{J}$ at different reduced temperatures T^* ($= T/(\varepsilon/k)$) that $\mathcal{J}$ is very insensitive to changes in T^* and hence to changes in ε as well. As a matter of fact a change of as much as 15% in ε at room temperature causes a change of as little as 1% in the values of $\mathcal{J}$ for H_2 - Kr and H_2 - Xe. Therefore no appreciable error is introduced in using the value of $\mathcal{J}$ obtained from empirical value for ε for the mixtures.

TABLE X

Lennard-Jones intermolecular separations σ for H_2-Kr and H_2-Xe pairs

Mixture	σ (calculated from profile analysis) Å	σ (empirical) $\sigma=(\sigma_1+\sigma_2)/2$ Å
H_2-Kr	3.02	3.26
H_2-Xe	3.23	3.53

APPENDIX I

Program for the analysis of overlap profiles :

```
C       NON LINEAR L.S. FIT OF SYNTHETIC OVERLAP PROFILE TO
C       EXPERIMENTAL OVERLAP PROFILE AND THEIR ANALYSIS
C       SUBROUTINE DRS READS RELATIVE LINE STRENGTHS AND THE
C       LINE FREQUENCIES, ONE DATA TO A CARD, COL 1-10,LINE STRENGTH
C       COL 11-20, LINE FREQUENCY
C       SUBROUTINE DREAD READS FREQUENCY AND INTENSITY OF THE
C       EXPERIMENTAL PROFILES. ONE DATA TO A CARD, COL 1-10
C       FREQUENCY, COL 11-20 RELATIVE INTENSITY IN TERMS OF
C       LOG10(I1/I2). AO= APPROX. INTENSITY OF Q(1),BO= APPROX.
C       VALUE OFINTER COL. HALF-WIDTH, D= APPROX. VALUE OF
C       INTRA COL. HALF WIDTH.
C       EPS= PRECISION REQ. IN AO,BO,AND D. H = INCREAMENT FOR DIFF.
        COMMON X(500),Y(500),N,S(99),SF(99),NL
        DIMENSION AY(500)
        DIMENSION Z(20)
    2   CALL DRS
    5   READ 10,Z
        PRINT 11,Z
   10   FORMAT(20A4)
   11   FORMAT(1H1,20A4//)
        CALL DREAD
        DO 340 I=1,N
  340   AY(I)=Y(I)
C       LS=0, ANOTHER DATA SET OF SAME BAND
C       LS = ANY POSITIVE NO. NEW DATA SET
C       LS = ANY NEGATIVE NO. END OF ENTIRE DATA SET
    1   READ 20,AO,BO,D,H,EPS,LS
   20   FORMAT(5F10.0,2I5)
        CALL CONVRT
        DO 200 K=1,15
        C1=0.
        C2=0.
        C3=0.
        C4=0.
        C5=0.
        C6=0.
        R1=0.
        R2=0.
        R3=0.
        DO 300 I=1,N
        CALL CAL(I,AO,BO,D,AF)
        CALL CAL(I,AO+H,BO,D,D1)
        CALL CAL(I,AO,BO+H,D,D2)
        CALL CAL(I,AO,BO,D+H,D3)
        DF1=(D1-AF)/H
        DF2=(D2-AF)/H
        DF3=(D3-AF)/H
        C1=C1+DF1*DF1
        C2=C2+DF1*DF2
        C3=C3+DF1*DF3
```

```
      C4=C4+DF2*DF2
      C5=C5+DF2*DF3
      C6=C6+DF3*DF3
      R0=Y(I)-AF
      R1=R1+R0*DF1
      R2=R2+R0*DF2
      R3=R3+R0*DF3
  300 CONTINUE
      ANU=C1*(C4*C6-C5*C5)+C2*(C3*C5-C2*C6)+C3*(C2*C5-C3*C4)
      A1=R1*(C4*C6-C5*C5)+C2*(R3*C5-R2*C6)+C3*(R2*C5-R3*C4)
      B1=C1*(R2*C6-R3*C5)+R1*(C5*C3-C2*C6)+C3*(C2*R3-C3*R2)
      DI=C1*(C4*R3-C5*R2)+C2*(C3*R2-C2*R3)+R1*(C2*C5-C3*C4)
      A1=A1/ANU
      B1=B1/ANU
      DI=DI/ANU
      A0=A0+A1
      B0=B0+B1
      D=D+DI
      PRINT 909,A0,B0,D,K
  909 FORMAT(3E20.7,I4)
      IF(ABS(A1)-EPS) 400,400,401
  400 IF(ABS(B1)-EPS) 403,403,401
  403 IF(ABS(DI)-EPS) 402,402,401
  401 CONTINUE
  200 CONTINUE
  402 PRINT 500,A0,B0,D
  500 FORMAT(5X,' HEIGHT='E15.7/6X,'     DQ='E15.7/6X,'     DC='E15.7//)
      DO 30 I=1,N
      CALL CAL(I,A0,B0,D,AF)
      RDN=X(I)
      Y(I)=AY(I)
      AF=AF*RDN
      DIFF=Y(I)-AF
      PRINT 31,X(I),Y(I),AF,DIFF
   31 FORMAT(F20.4,3F20.6)
   30 CONTINUE
      PRINT 19
   19 FORMAT(//)
      DO 707 J=3900,5000,20
      AX=J
      FN=0.
      DO 708 I=1,NL
      R=4.828210053E-03
      RN=A0*S(I)*(1.-1./(1.+((AX-SF(I))*1./B0)**2))
      XT=AX-SF(I)
      XT=XT/D
      CALL BESM2(XT,RES)
      RN=RN*RES
      IF(AX-SF(I)) 799,800,800
  799 RN=RN*EXP(-R*(SF(I)-AX))
  800 FN=FN+RN
```

```
  708 CONTINUE
      FN=FN*AX
      PRINT 828,AX,FN
  828 FORMAT(F10.4,5X,E20.8)
  707 CONTINUE
      CALL PLOT(AO,BO,D)
      IF(LS) 50,5,2
   50 CALL EXIT
      END

      SUBROUTINE DREAD
      COMMON X(500),Y(500),N,S(99),SF(99),NL
      N=0
      DO 201 J=1,500
      READ 300,X(J),Y(J),LAST
300   FORMAT(2F10.0,I5)
      N=N+1
      IF(LAST) 100,201,100
  201 CONTINUE
  100 RETURN
      END

      SUBROUTINE DRS
      COMMON X(500),Y(500),N,S(99),SF(99),NL
  100 NL=0
      DO 21 J=1,99
      READ 31,S(J),SF(J),LAST
   31 FORMAT(2F10.0,I5)
      NL=NL+1
      IF(LAST) 11,21,11
   21 CONTINUE
   11 RETURN
      END

      SUBROUTINE CAL(J,AL,BE,DE,FN)
      COMMON X(500),Y(500),N,S(99),SF(99),NL
      FN=0.
      DO 220 I=1,NL
      R=4.828210053E-03
      RN=AL*S(I)*(1.-1./(1.+((X(J)-SF(I))/BE)**2))
      XT=X(J)-SF(I)
      XT=XT/DE
      CALL BESM2(XT,RES)
      RN=RN*RES
      IF(X(J)-SF(I)) 199,200,200
  199 RN=RN*EXP(-R*(SF(I)-X(J)))
  200 FN=FN+RN
  220 CONTINUE
      RETURN
      END
```

```
      SUBROUTINE CONVRT
      COMMON X(500),Y(500),N,S(99),SF(99),NL
      DO 250 I=1,N
      Y(I)=Y(I)/X(I)
  250 CONTINUE
      RETURN
      END

      SUBROUTINE BESM2(X1,RES)
C     THIS SUBROUTINE CALCULATES MOD. BESSEL FN OF THE 2ND KIND OF ORDER 2
      DOUBLE PRECISION T,AI,AI1,AB1,X,AB2,XR
      X=ABS(X1)
      IF(X.GT.0.) GO TO 200
      RES=2.0000000
      RETURN
  200 IF(X.GT.2.) GO TO 400
      T=X/3.75
      AI=1.+3.5156229*T**2+3.0899424*T**4+1.2067492*T**6+.2659732*T**8
     1 +.0360768*T**10+.0045813*T**12
      AI1=.5+.87890594*T**2+.51498869*T**4+.15084934*T**6+.02658733*T**8
     1+.00301532*T**10+.00032411*T**12
      XR=X/2.
      AB1=              +1.+.15443144*XR**2-.67278579*XR**4
     1 -.18156897*XR**6-.01919402*XR**8-.00110404*XR**10
     2 -.00004686*XR**12
     3+X**2*DLOG(XR)*AI1
      AB1=AB1*2.
      AB2=-AI*DLOG(XR) -.57721566+.42278420*XR**2+.23069756*XR**4
     1+.03488590*XR**6+.00262698*XR**8+.00010750*XR**10+.00000740*XR**12
      RES=AB1+AB2*X**2
      RETURN
  400 XR= 2./X
      AB1=1.25331414+.23498619*XR-.03655620*XR**2+.01504268*XR**3
     1 -.00780353*XR**4+.00325614*XR**5-.00068245*XR**6
      AB1=2.*AB1*X**.5*DEXP(-1.*X )
      AB2=1.25331414-.07832358*XR+.02189568*XR**2-.01062446*XR**3
     1 +.00587872*XR**4-.00251540*XR**5+.00053208*XR**6
      AB2=AB2*X**1.5*DEXP(-1.*X)
      RES = AB1+AB2
      RETURN
      END

      SUBROUTINE PLOT(AR,BR,DR)
      COMMON X(500),Y(500),N,S(99),SF(99),NL
C     THIS PROGRAM PLOTS INDIVIDUAL LINE PROFILES
      R=4.828210053E-03
      PRINT 900
  900 FORMAT(1H1)
      DO 301 I=1,NL
      J=SF(I)-500.
      K=SF(I)+1000.
```

```
      DO 300 L=J,K,10
      AL=L
      FN=AR*S(I)*(1.-1./(1.+((AL-SF(I))/BR)**2))
      X1=(SF(I)-AL)/DR
      CALL BESM2(X1,RES)
      FN=FN*RES*AL
      IF(AL-SF(I)) 1401,1400,1400
1401  FN=FN*EXP(-R*(SF(I)-AL))
1400  PRINT 1420, AL,FN,SF(I)
1420  FORMAT(F10.4,E20.8,F15.4)
 300  CONTINUE
      PRINT 19
  19  FORMAT(1H1)
 301  CONTINUE
      RETURN
      END
```

A computer plot of the line-form used for the overlap component in the present analysis (inter- and intra- collisional width-parameters have arbitrarily been assumed as 100 and 50 wave numbers, respectively) :

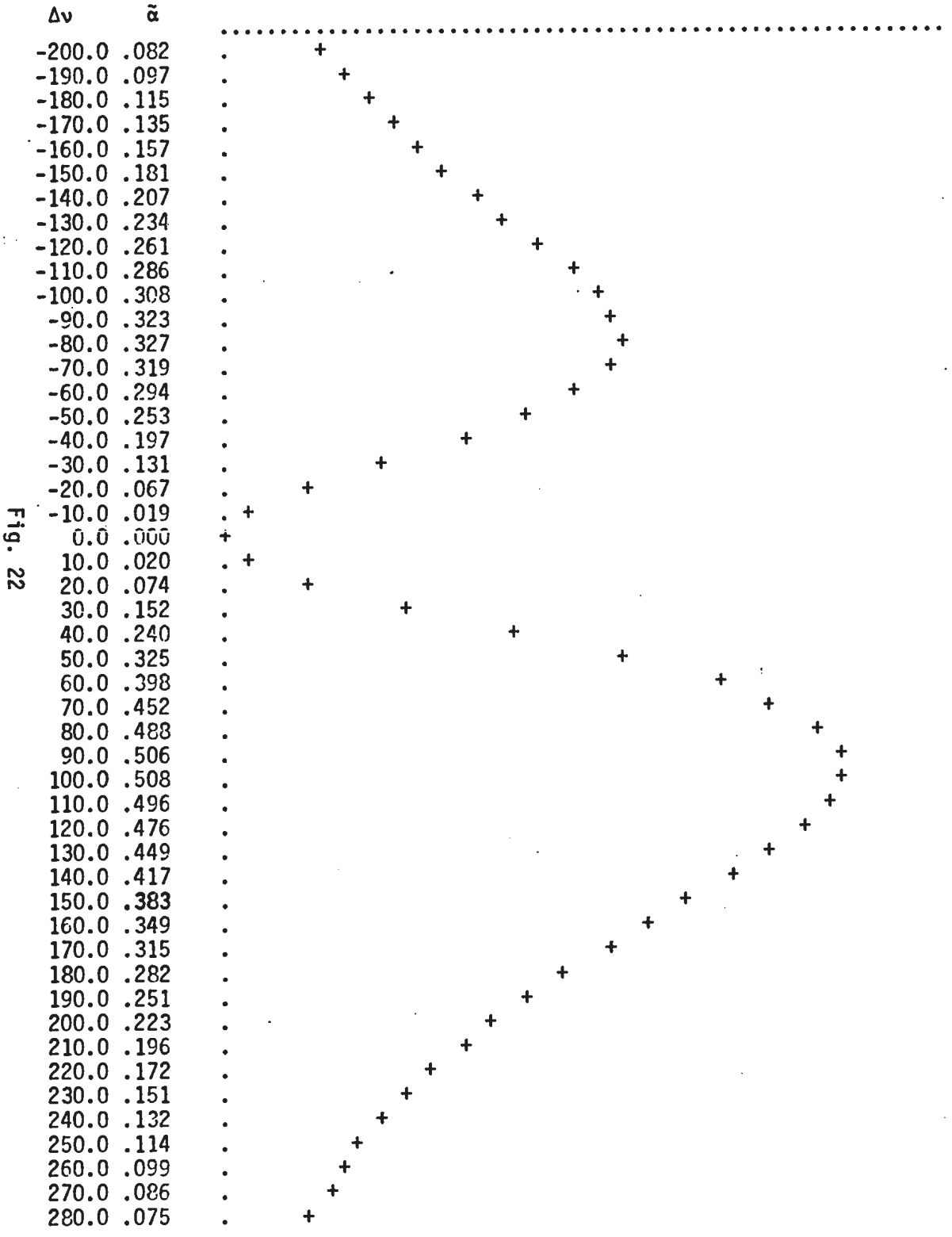

Fig. 22

APPENDIX II

Program for calculating the synthetic quadrupolar profiles :

```
C      NON LINEAR L.S. FIT OF SYNTHETIC QUADRUPOLAR PROFILE
C      TO EXPERIMENTAL PROFILE AND ANALYSIS OF QUAD. PART
C      SUBROUTINE DRS READS RELATIVE LINE STRENGTHS AND THE
C      LINE FREQUENCIES, ONE DATA TO A CARD, COL 1-10,LINE STRENGTH
C      COL 11-20, LINE FREQUENCY
C      SUBROUTINE DREAD READS FREQUENCY AND INTENSITY OF THE
C      EXPERIMENTAL PROFILES. ONE DATA TO A CARD, COL 1-10
C      FREQUENCY, COL 11-20 RELATIVE INTENSITY IN TERMS OF
C      LOG10(I1/I2).
C      AO= APPROX. INTENSITY OF S(1), BO= APPROX. VALUE OF
C      QUADRUPOLAR HALF WIDTH, EPS= PRECISION REQUIRED IN
C      AO AND BO. H= INCREAMENT FOR DIFFERENTIATION
C      FINAL ITERATED VALUE OF AO,BO ARE PRINTED AND EXP.
C      AND CAL. VALUES OF INTENSITY ARE PRINTED
       COMMON X(500),Y(500),N,S(99),SF(99),NL
       DIMENSION AY(500)
       DIMENSION Z(20)
     2 CALL DRS
     5 READ 10,Z
       PRINT 11,Z
    10 FORMAT(20A4)
    11 FORMAT(1H1,20A4//)
       CALL DREAD
     1 READ 20,AO,BO,D,H,EPS,LS
    20 FORMAT(5F10.0,2I5)
       DO 340 IS=1,N
   340 AY(IS)=Y(IS)
       DO 1944 IK=1,NL
       SF(IK)=SF(IK)+1.
  1944 CONTINUE
       DO 733 IA=1,14
       CALL CONVRT
       DO 734 K=1,NL
       SF(K)=SF(K)-1.
   734 CONTINUE
       IAA=IA-1
       PRINT 1320,IAA
  1320  FORMAT(/5X,'FREQUENCY SHIFT ='I2/)
       DO 200 K=1,40
       C1=0.
       C2=0.
       C3=0.
       C4=0.
       C5=0.
       C6=0.
       DO 300 I=1,N
       CALL CAL(I,AO,BO,D,AF)
       CALL CAL(I,AO+H,BO,D,D1)
```

```
      CALL CAL(I,AO,BO+H,D,D2)
      DF1=(D1-AF)/H
      DF2=(D2-AF)/H
      C1=C1+DF1*DF1
      C2=C2+DF1*DF2
      C3=C2
      C4=C4+DF2*DF2
      R=Y(I)-AF
      C5=C5+R*DF1
  300 C6=C6+R*DF2
      A1=(C5*C4-C6*C2)/(C1*C4-C3*C2)
      B1=(C1*C6-C5*C3)/(C1*C4-C3*C2)
      AO=AO+A1
      BO=BO+B1
      IF(ABS(A1)-EPS) 400,400,401
  400 IF(ABS(B1)-EPS) 402,402,401
  401 CONTINUE
  200 CONTINUE
  402 PRINT 500,AO,BO,D
  500 FORMAT(3E20.8//)
      DO 30 I=1,N
      CALL CAL(I,AO,BO,D,AF)
      RDN=X(I)
      Y(I)=AY(I)
      AF=AF*RDN
      DIFF=Y(I)-AF
      PRINT 31,X(I),Y(I),AF,DIFF
   31 FORMAT(F20.4,3F20.6)
   30 CONTINUE
      PRINT 19
   19 FORMAT(//)
      DO 707 J= 3500,5500,20
      AX=J
      FN=0.
      DO 708 I=1,NL
      R=4.828210053E-03
      RN=(AO*S(I))/(((AX-SF(I))/BO)**2+1.)
      IF(AX-SF(I)) 799,800,800
  799 RN=RN*EXP(-R*(SF(I)-AX))
  800 FN=FN+RN
  708 CONTINUE
      FN=FN*AX
      PRINT 828,AX,FN
  828 FORMAT(F10.4,5X,E20.8)
  707 CONTINUE
      PRINT 19
      CALL PLOT(AO,BO,D)
  733 CONTINUE
      DO 833 K=1,NL
      SF(K)=SF(K)+13.
```

```
833 CONTINUE
    IF(LS) 50,5,50
 50 CALL EXIT
    END

    SUBROUTINE DREAD
    COMMON X(500),Y(500),N,S(99),SF(99),NL
    N=0
    DO 201 J=1,500
    READ 300,X(J),Y(J),LAST
300 FORMAT(2F10.0,I5)
    N=N+1
    IF(LAST) 100,201,100
201 CONTINUE
100 RETURN
    END

    SUBROUTINE DRS
    COMMON X(500),Y(500),N,S(99),SF(99),NL
100 NL=0
    DO 21 J=1,99
    READ 31,S(J),SF(J),LAST
 31 FORMAT(2F10.0,I5)
    NL=NL+1
    IF(LAST) 11,21,11
 21 CONTINUE
 11 RETURN
    END

    SUBROUTINE CAL(J,AL,BE,DE,FN)
    COMMON X(500),Y(500),N,S(99),SF(99),NL
    FN=0.
    DO 220 I=1,NL
    R=4.828210053E-03
    RN=(AL*S(I))/(((X(J)-SF(I))/BE)**2+1.)
    IF(X(J)-SF(I)) 199,200,200
199 RN=RN*EXP(-R*(SF(I)-X(J)))
200 FN=FN+RN
220 CONTINUE
    RETURN
    END

    SUBROUTINE PLOT(AR,BR,DR)
    COMMON X(500),Y(500),N,S(99),SF(99),NL
    R=4.828210053E-03
    PRINT 900
900 FORMAT(1H1)
    DO 301 I=1,NL
    J=SF(I)-1000.
    K=SF(I)+1000.
```

```
      DO 300 L=J,K,10
      AJ=L
      STR=(AR*S(I))/(((AJ-SF(I))/BR)**2+1.)
      STR=STR*AJ
      IF(AJ-SF(I)) 401,400,400
  401 STR=STR*EXP(-R*(SF(I)-AJ))
  400 PRINT 420,AJ,STR,SF(I)
  420 FORMAT(F10.4,E20.8,5X,F10.4)
  300 CONTINUE
      PRINT 21
   21 FORMAT(//)
  301 CONTINUE
      RETURN
      END

      SUBROUTINE CONVRT
      COMMON X(500),Y(500),N
      DO 250 I=1,N
      Y(I)=Y(I)/X(I)
  250 CONTINUE
      RETURN
      END
```

A RESEARCH PUBLICATION BY THE AUTHOR

G. Varghese, S.N. Ghosh, and S. Paddi Reddy: "Frequency shifts of quadrupolar components of the collision-induced fundamental band of H_2" Journal of Molecular Spectroscopy (in press).

ACKNOWLEDGMENTS

The author wishes to express his sincere gratitude to his supervisor Dr. S.P. Reddy, for initiating this project, continuous guidance throughout the research work, helpful criticism and encouragement.

The author would like to thank Dr. G. Varghese for assisting with the experiments and rendering valuable suggestions. Thanks are also due to Dr. M. J. Clouter in connection with the use of liquid helium cryostat for the preparation of parahydrogen, and to Dr. M. Lal of Mathematics Department for many helpful discussions regarding computer procedures.

The author is grateful to the Newfoundland and Labrador Computer Services Ltd. for the efficient handling of the computer programs.

The financial support received in the form of research fellowships from Memorial University of Newfoundland and from Dr. Reddy's N.R.C. operating grant A-2440 is gratefully acknowledged.

REFERENCES

1. Birnbaum, A. and Poll, J.D.,J. Atmos. Sci. 26, 943(1969).
2. Bishop, R.B. M.Sc.,Thesis(1966), Memorial Univ. of Nfld.
3. Bosomworth, D.R. and Gush, H.P.,Can. J. Phys. 43, 751(1965).
4. Bridge, N.J. and Buckingham, A.D.,J. Chem. Phys. 40, 2733(1964).
5. Chang, K.S. M.Sc.,Thesis(1971), Memorial Univ. of Nfld.
6. Chisholm, D.A. and Welsh, H.L.,Can. J. Phys. 32, 291(1954).
7. Crawford, M.F., Welsh, H.L. and Locke, J.L.,Phys. Rev. 75, 1607(1949).
8. Hare, W.F. and Welsh, H.L.,Can. J. Phys. 36, 88(1958).
9. Hirschfelder, J.O., Curtiss, C.F. and Bird, R.B.,1967, Molecular Theory of Gases and Liquids, 2nd Edition(Wiley,N.Y.).
10. Humphreys, C.J.,J. Opt. Soc. Am. 43, 1027(1953).
11. Hunt, J.L.,Ph.D. Thesis(1959), Univ. of Toronto.
12. Hunt, J.L. and Welsh, H.L.,Can. J. Phys. 42, 873(1964).
13. I.U.P.A.C. 1961. Tables of Wave Numbers for the Calibration of Infrared Spectrometers(Butterworth's,London).
14. Karl, G. and Poll, J.D.,J. Chem. Phys. 46, 2944(1967).
15. Kiss, Z.J. and Welsh, H.L.,Can. J. Phys. 37, 1249(1959).
16. Kolos, W. and Wolniewicz, L.J., J. Chem. Phys. 46, 1426(1967).
17. Kuo, C.Z., M.Sc. Thesis(1970), Memorial Univ. of Nfld.
18. Levine, H.B. and Birnbaum, G.,Phys. Rev. 154, 86(1967).
19. Mactaggart, J.W. and Hunt, J.L.,Can. J. Phys. 47, 51(1969).
20. Michels, A., Boltzen, A., Friedman, A.S. and Sengers, J.V., Physica, 22, 121(1956).
21. Michels, A., De Graaff, W. and Ten Seldam, C.A.,Physica, 20, 99(1954).

22. Michels, A., De Graaff, W., Wassenaar, T., Levelt, J.M.H. and Louwerse, P., Physica, 25, 25(1959).

23. Michels, A., Wassenaar, T. and Louwerse, P.,Physica, 20, 99(1954).

24. Plyler, E.K., Blaine, L.R. and Nowak, M.J., J. Res. Natl. Bur. Stds. 58, 195(1957).

25. Reddy, S.P. and Cho, C.W., Can. J. Phys. 43, 793(1965).

26. Reddy, S.P. and Cho, C.W., Can. J. Phys. 43, 2331(1965).

27. Reddy, S.P. and Kuo, C.Z., J. Mol. Spec. 37, 327(1971).

28. Reddy, S.P. and Lee, W.F., Can. J. Phys. 46, 1373(1968).

29. Schmauch, G.E. and Singleton, A.H., Ind. Engr. Chem. 56, 20(1964).

30. Sears, V.F., Can. J. Phys. 46, 1163(1968).

31. Sears, V.F., Can. J. Phys. 46, 2315(1968).

32. Stoicheff, B.P., Can. J. Phys. 35, 730(1957).

33. Trappeniers, N.J., Wassenaar, T. and Wolkers, G.J., Physica, 32, 1503(1966).

34. Van Kranendonk, J., Physica, 23, 825(1957).

35. Van Kranendonk, J., Physica, 24, 347(1958).

36. Van Kranendonk, J., Can. J. Phys. 46, 1173(1968).

37. Van Kranendonk, J. and Kiss, Z.J., Can. J. Phys. 37, 1187(1959).

38. Varghese, G. and Reddy, S.P., Can. J. Phys. 47, 2745(1969).

39. Watanabe, A., Can. J. Phys. 49, 1320(1971).

40. Watanabe, A. and Welsh, H.L., Can. J. Phys. 43, 818(1965).

41. Watanabe, A. and Welsh, H.L., Can. J. Phys. 45, 2857(1967).

42. Welsh, H.L., Crawford, M.F. and Locke, J.L., Phys. Rev. 75, 850(1949).